

A Search for Squarks of R-parity Violating SUSY at HERA

H1 Collaboration

Abstract

A search for squarks of R-parity violating supersymmetry is performed in ep collisions at HERA using H1 1994 e^+ data. Direct single production of squarks of each generation by e^+ -quark fusion via a Yukawa coupling λ^0 is considered. All possible R-parity violating decays and gauge decays of the squarks are taken into account. No significant deviation from the Standard Model predictions is found in the various multi-lepton and multi-jet final states studied and exclusion limits are derived. At 95% confidence level, the existence of first generation squarks is excluded for masses up to 240 GeV for coupling values $\lambda^0 \leq \sqrt{4\pi\alpha_{em}}$. The limits obtained are shown to be only weakly dependent on the free parameters of the Minimal Supersymmetric Standard Model. Stop squarks are excluded for masses up to 138 GeV for coupling $\lambda^0 \cos \theta_t$ to e^+d pairs & $0.1 \sqrt{4\pi\alpha_{em}}$, where θ_t is the mass mixing angle.

Light stop squarks are furthermore searched for through pair production in gg -gluon fusion processes. No signal is observed and exclusion limits are derived. Masses in the range 9 to 244 GeV are excluded at 95% confidence level for $\lambda^0 \cos \theta_t > 10^{-4}$.

S. Aidi¹⁴, V. Andreev²⁶, B. Andrieu²⁹, R. D. Appuhn¹², M. Aipagaus³⁷, A. Babaev²⁵,
 J. Bahr³⁶, J. Ban¹⁸, Y. Ban²⁸, P. Baranov²⁶, E. Barrelet³⁰, R. Barschke¹², W. Bartel¹²,
 M. Barth⁵, U. Bassler³⁰, H. P. Beck³⁸, H.-J. Behrend¹², A. Belusov²⁶, Ch. Berger¹,
 G. Bernardi³⁰, R. Bernet³⁷, G. Bertrand-Coremans⁵, M. Besancon¹⁰, R. Beyer¹²,
 P. Biddulph²³, P. Bispham²³, J. C. Bizot²⁸, V. Blobel¹⁴, K. Borras⁹, F. Botterweck⁵,
 V. Boudry²⁹, A. Braemer¹⁵, W. Braunschweig¹, V. Brisson²⁸, P. Buef²⁹, D. Bruncko¹⁸,
 C. Bune¹⁶, R. Buchholz¹², L. Bungener¹⁴, J. Burger¹², F. W. Busser¹⁴, A. Buniatian^{12;39},
 S. Burke¹⁹, M. J. Burton²³, G. Buschhorn²⁷, A. J. Campbell¹², T. Carli²⁷, F. Charles¹²,
 M. Charlet¹², D. Clarke⁶, A. B. Clegg¹⁹, B. Clerbaux⁵, S. Cocks²⁰, J. G. Contreras⁹,
 C. Cormack²⁰, J. A. Coughlan⁶, A. Courau²⁸, M.-C. Cousinou²⁴, G. Cozzika¹⁰,
 L. Criegee¹², D. G. Cussans⁶, J. Cvach³¹, S. Dagoret³⁰, J. B. Dainton²⁰, W. D. Dau¹⁷,
 K. Daum³⁵, M. David¹⁰, C. L. Davis¹⁹, B. Delcourt²⁸, A. De Roeck¹², E. A. De Wolf⁶,
 M. Dirkmann⁹, P. Dixon¹⁹, P. DiNezza³³, W. Dlugosz⁸, C. Döllfus³⁸, J. D. Dowell⁴,
 H. B. Dreis², A. Drouskoff²⁵, D. Dullmann¹⁴, O. Dünge¹⁴, H. Dühm¹³, J. Ebert³⁵,
 T. R. Ebert²⁰, G. Eckerlin¹², V. Efremenko²⁵, S. Egl³⁸, R. Eichler³⁷, F. Eisele¹⁵,
 E. Eisenhandler²¹, R. J. Ellison²³, E. Elsen¹², M. Erdmann¹⁵, W. Erdmann³⁷, E. Evrard⁵,
 A. B. Fahr¹⁴, L. Favart²⁸, A. Fedotov²⁵, D. Feeken¹⁴, R. Felst¹², J. Feltesse¹⁰,
 J. Ferencel¹⁸, F. Ferrarotto³³, K. Flamm¹², M. Fleischer⁹, M. Fliesser²⁷, G. Flugge²,
 A. Fomchenko²⁶, B. Fominykh²⁵, J. Formanek³², J. M. Foster²³, G. Franke¹²,
 E. Fretwurst¹³, E. Gabathuler²⁰, K. Gabathuler³⁴, F. Gaede²⁷, J. Garvey⁴, J. Gayler¹²,
 M. Gebauer³⁶, A. Gellrich¹², H. Genzel¹, R. Gerhards¹², A. Glazov³⁶, U. Gohlach¹²,
 L. Gohlisch⁷, N. Gogitidze²⁶, M. Goldberg³⁰, D. Goldner⁹, K. Golec-Biat⁷,
 B. Gonzalez-Pineiro³⁰, I. Gorelov²⁵, C. Grab³⁷, H. Grassler², R. Grassler²,
 T. Greenshaw²⁰, R. Grieths²¹, G. G. Rindhammer²⁷, A. Gruber²⁷, C. Gruber¹⁷,
 J. Haack³⁶, D. Haidt¹², L. Hajduk⁷, M. Hampel¹, W. J. Haynes⁶, G. Heinzelmann¹⁴,
 R. C. W. Henderson¹⁹, H. Henschel³⁶, I. Herynek³¹, M. F. Hess²⁷, W. Hildesheim¹²,
 K. H. Hiller³⁶, C. D. Hilton²³, J. Hladky³¹, K. C. Hoeger²³, M. Hoppner⁹, D. Homann¹²,
 T. Holtom²⁰, R. Horisberger³⁴, V. L. Hudgson⁴, M. Hutte⁹, H. Hufnagel¹⁵, M. Ibbotson²³,
 H. Iitterbeck¹, A. Jacholkowska²⁸, C. Jacobsson²², M. Jare²⁸, J. Janoth¹⁶, T. Jansen¹²,
 L. Jonsson²², K. Johannsen¹⁴, D. P. Johnson⁵, L. Johnson¹⁹, H. Jung¹⁰, P. J. P. Kalms²¹,
 M. Kander¹², D. Kant²¹, R. Kaschowitz², U. Kathage¹⁷, J. Katzy¹⁵, H. H. Kaufmann³⁶,
 O. Kaufmann¹⁵, S. Kazarian¹², I. R. Kenyon⁴, S. Kemiche²⁴, C. Keuker¹, C. Kiesling²⁷,
 M. Klein³⁶, C. Kleinwort¹², G. Knies¹², T. Kohler¹, J. H. Kohne²⁷, H. Kolanoski³,
 F. Kole⁸, S. D. Kolya²³, V. Korbel¹², M. Kom⁹, P. Kostka³⁶, S. K. Kotelnikov²⁶,
 T. Kramerer⁹, M. W. Krasny^{7;30}, H. Krehbiel¹², D. Kruker², U. Kuger¹²,
 U. Kruener-Markus¹², H. Kuster²², M. Kühlen²⁷, T. Kurca³⁶, J. Kurzhofer⁹, D. Lacour³⁰,
 B. Laforge¹⁰, R. Lander⁸, M. P. J. Landon²¹, W. Lange³⁶, U. Langenegger³⁷,
 J.-F. Laporte¹⁰, A. Lebedev²⁶, F. Lehner¹², C. Leverenz¹², S. Levonian²⁹, Ch. Ley²,
 G. Lindstrom¹³, M. Lindstrom²², J. Link⁸, F. Linsel¹², J. Lipinski¹⁴, B. List¹²,
 G. Lobo²⁸, H. Lohmeyer²², J. W. Lomas²³, G. C. Lopez¹³, V. Lubimov²⁵, D. Luke^{9;12},
 N. Magnussen³⁵, E. Malinowski²⁶, S. Mani⁸, R. Maracek¹⁸, P. Marage⁵, J. Marks²⁴,
 R. Marshall²³, J. Martens³⁵, G. Martin¹⁴, R. Martin²⁰, H.-U. Martyn¹, J. Martyniak⁷,
 T. Mavroidis²¹, S. J. Maxwell²⁰, S. J. McMahon²⁰, A. Mehta⁶, K. Meier¹⁶, T. Merz³⁶,
 A. Meyer¹⁴, A. Meyer¹², H. Meyer³⁵, J. Meyer¹², P.-O. Meyer², A. Migliorini⁹,
 S. Mikocki⁷, D. Milsch²⁰, J. Moerk²⁷, F. Moreau²⁹, J. V. Morris⁶, E. Mroczko⁷,

D. Müller³⁸, G. Müller¹², K. Müller¹², P. Murri⁸, V. Nagovizin²⁵, R. Nahnauer³⁶,
 B. Naroska¹⁴, Th. Naumann³⁶, P. R. Newman⁴, D. Newton¹⁹, D. Neyret³⁰,
 H. K. Nguyen³⁰, T. C. Nicholls⁴, F. Niebergall¹⁴, C. Niebuhr¹², Ch. Niedzballa¹,
 H. Niggli³⁷, R. Nisius¹, G. Nowak⁷, G. W. Noyes⁶, M. Nyberg-Werther²², M. O'Kuden²⁰,
 H. Oberlack²⁷, U. Obrock⁹, J. E. Olsson¹², D. Ozerov²⁵, P. Palmén², E. Panaro¹²,
 A. Panitch⁵, C. Pascaud²⁸, G. D. Patel²⁰, H. Pawletta², E. Peppel³⁶, E. Perez¹⁰,
 J. P. Phillips²⁰, A. Pichot²⁴, D. Pitzl³⁷, G. Pope⁸, S. Prell¹², R. Prosi¹², K. Rabbertz¹,
 G. Radel¹², F. Raupach¹, P. Reimer³¹, S. Reinshagen¹², H. Rick⁹, V. Ried¹³,
 J. Riedberger³⁷, F. Riepenhausen², S. Ries¹⁴, E. Rizvi²¹, S. M. Robertson⁴,
 P. Robmann³⁸, H. E. Robo³⁶, R. Roosen⁵, K. Rosenbauer¹, A. Rostovtsev²⁵, F. Rouse⁸,
 C. Royon¹⁰, K. Ruter²⁷, S. Rusakov²⁶, K. Rybicki⁷, N. Sahm², D. P. C. Sankey⁶,
 P. Schacht²⁷, S. Schiek¹⁴, S. Schleich⁶, P. Schlexer¹⁵, W. von Schlippe²¹, D. Schmidt³⁵,
 G. Schmidt¹⁴, A. Schoning¹², V. Schröder¹², E. Schuhmann²⁷, B. Schwab¹⁵, F. Seifow¹²,
 M. Seidel¹³, R. Sell¹², A. Semenov²⁵, V. Shekelyan¹², I. Sheviakov²⁶, L. N. Shtarkov²⁶,
 G. Siegmund¹⁷, U. Siewert¹⁷, Y. Sirois²⁹, I. O. Skillicorn¹¹, P. Smirnov²⁶, J. R. Smith⁸,
 V. Solochenko²⁵, Y. Soloviev²⁶, A. Specka²⁹, J. Spiekermann⁹, S. Spielmann²⁹,
 H. Spitzer¹⁴, F. Squinabol²⁸, R. Starosta¹, M. Steenbock¹⁴, P. Stein¹², R. Steinberg²,
 H. Steiner^{12;40}, B. Stella³³, A. Stellberger¹⁶, J. Stier¹², J. Stiewe¹⁶, U. Stöcklein³⁶,
 K. Stolze³⁶, U. Straumann³⁸, W. Struczkowski², J. P. Sutton⁴, S. Tapprogge¹⁶,
 M. Tasevsky³², V. Tchernyshov²⁵, S. Tchetchelnitski²⁵, J. Theissen², C. Thiebaux²⁹,
 G. Thompson²¹, P. Türol³⁸, J. Tumau⁷, J. Tutas¹⁵, P. Uelkes², A. Uslak²⁶, S. Valkar³²,
 A. Valkarova³², C. Vallee²⁴, D. Vandenplas²⁹, P. Van Esch⁵, P. Van Mechelen⁵,
 Y. Vazdik²⁶, P. Verrecchia¹⁰, G. Villet¹⁰, K. Wacker⁹, A. Wagners², M. Wagners³⁴,
 A. Walther⁹, B. Wauth²³, G. Weber¹⁴, M. Weber¹², D. Wegener⁹, A. Wegner²⁷,
 T. Wengler¹⁵, M. Werner¹⁵, L. R. West⁴, T. Wilksen¹², S. Willard⁸, M. Winder³⁶,
 G. W. Winter¹², C. Wittke¹⁴, E. Wunsch¹², J. Zacek³², D. Zarbock¹³, Z. Zhang²⁸,
 A. Zhokin²⁵, M. Zimmer¹², F. Zomer²⁸, J. Zsembory¹⁰, K. Zuber¹⁶, and M. Zurborg³⁸

¹ I. Physikalisches Institut der RWTH, Aachen, Germany^a

² III. Physikalisches Institut der RWTH, Aachen, Germany^a

³ Institut für Physik, Humboldt-Universität, Berlin, Germany^a

⁴ School of Physics and Space Research, University of Birmingham, Birmingham, UK^b

⁵ Inter-University Institute for High Energies ULB-VUB, Brussels; Universitaire Instelling Antwerpen, Wilrijk; Belgium^c

⁶ Rutherford Appleton Laboratory, Chilton, Didcot, UK^b

⁷ Institute for Nuclear Physics, Cracow, Poland^d

⁸ Physics Department and IIRPA, University of California, Davis, California, USA^e

⁹ Institut für Physik, Universität Dortmund, Dortmund, Germany^a

¹⁰ CEA, DSM/DAPNIA, CE-Saclay, Gif-sur-Yvette, France

¹¹ Department of Physics and Astronomy, University of Glasgow, Glasgow, UK^b

¹² DESY, Hamburg, Germany^a

¹³ I. Institut für Experimentalphysik, Universität Hamburg, Hamburg, Germany^a

¹⁴ II. Institut für Experimentalphysik, Universität Hamburg, Hamburg, Germany^a

¹⁵ Physikalisches Institut, Universität Heidelberg, Heidelberg, Germany^a

¹⁶ Institut für Hochenergiephysik, Universität Heidelberg, Heidelberg, Germany^a

- ¹⁷ Institut für Reine und Angewandte Kernphysik, Universität Kiel, Kiel, Germany^a
- ¹⁸ Institute of Experimental Physics, Slovak Academy of Sciences, Kosice, Slovak Republic^f
- ¹⁹ School of Physics and Chemistry, University of Lancaster, Lancaster, UK^b
- ²⁰ Department of Physics, University of Liverpool, Liverpool, UK^b
- ²¹ Queen Mary and Westfield College, London, UK^b
- ²² Physics Department, University of Lund, Lund, Sweden^g
- ²³ Physics Department, University of Manchester, Manchester, UK^b
- ²⁴ CPPM, Université d'Aix-Marseille II, IN2P3-CNRS, Marseille, France
- ²⁵ Institute for Theoretical and Experimental Physics, Moscow, Russia
- ²⁶ Lebedev Physical Institute, Moscow, Russia^f
- ²⁷ Max-Planck-Institut für Physik, München, Germany^a
- ²⁸ LAL, Université de Paris-Sud, IN2P3-CNRS, Orsay, France
- ²⁹ LPNHE, Ecole Polytechnique, IN2P3-CNRS, Palaiseau, France
- ³⁰ LPNHE, Universités Paris VI and VII, IN2P3-CNRS, Paris, France
- ³¹ Institute of Physics, Czech Academy of Sciences, Praha, Czech Republic^{f,h}
- ³² Nuclear Center, Charles University, Praha, Czech Republic^{f,h}
- ³³ INFN Roma and Dipartimento di Fisica, Università "La Sapienza", Roma, Italy
- ³⁴ Paul Scherrer Institut, Villigen, Switzerland
- ³⁵ Fachbereich Physik, Bergische Universität Gesamthochschule Wuppertal, Wuppertal, Germany^a
- ³⁶ DESY, Institut für Hochenergiephysik, Zeuthen, Germany^a
- ³⁷ Institut für Teilchenphysik, ETH, Zürich, Switzerlandⁱ
- ³⁸ Physik-Institut der Universität Zürich, Zürich, Switzerlandⁱ
- ³⁹ Visitor from Yerevan Phys. Inst., Armenia
- ⁴⁰ On leave from LBL, Berkeley, USA

^a Supported by the Bundesministerium für Forschung und Technologie, FRG, under contract numbers 6AC17P, 6AC47P, 6DO57I, 6HH17P, 6HH27I, 6HD17I, 6HD27I, 6K117P, 6MP17I, and 6WT87P

^b Supported by the UK Particle Physics and Astronomy Research Council, and formerly by the UK Science and Engineering Research Council

^c Supported by FNRS-NFWO, IISN-IKW

^d Supported by the Polish State Committee for Scientific Research, grant nos. 115/E-743/SPUB/P03/109/95 and 2P03B 244 08p01, and Stiftung für Deutsch-Polnische Zusammenarbeit, project no.506/92

^e Supported in part by USDOE grant DE-F603 91ER 40674

^f Supported by the Deutsche Forschungsgemeinschaft

^g Supported by the Swedish Natural Science Research Council

^h Supported by GACR, grant no. 202/93/2423, GAVCR, grant no. 19095 and GACR, grant no. 342

ⁱ Supported by the Swiss National Science Foundation

1 Introduction

The search for squarks, the scalar supersymmetric (SUSY) partners of the quarks, is especially promising at the ep collider HERA if they possess a lepton number violating Yukawa coupling κ_p^0 to lepton-quark pairs. Such squarks, present in the R-parity violating (\mathbb{R}_p) SUSY extension of the Standard Model (SM), can be singly produced via the coupling κ_p^0 as s-channel resonances. Masses up to the kinematic limit of $\sqrt{s} = 300$ GeV are accessible by the fusion of the 27.5 GeV initial state positron with a quark of the 820 GeV incoming proton. In the low mass range, pair production via γ -gluon fusion provides a complementary search largely insensitive to the Yukawa coupling.

In this paper, squarks are searched through single production via a \mathbb{R}_p coupling, considering both \mathbb{R}_p decays and all possible decays via gauge couplings involving mixed states of gauginos and higgsinos. A search for pair production of light stops at low masses via γ -gluon fusion is also carried out. The analysis uses the 1994 e^+p data corresponding to an integrated luminosity of $\mathcal{L}_{\text{data}} = 283 \text{ pb}^{-1}$. Earlier squark searches at HERA were presented in [1].

2 Phenomenology

The general SUSY superpotential allows for gauge invariant terms with Yukawa couplings between the scalar squarks (\tilde{q}) or sleptons (\tilde{l}) and the known SM fermions. Such couplings exist if one assumes the possibility of violating (multiplicatively) the conservation of R-parity which is imposed in the Minimal Supersymmetric Standard Model (MSSM); $R_p = (-1)^{3B + L + 2S}$ where S denotes the spin, B the baryon number and L the lepton number of the particles. Of particular interest for HERA are the \mathbb{R}_p terms $\kappa_{ijk}^0 \tilde{L}_i \tilde{Q}_j D_k$ of the superpotential which allow for lepton number violating processes. By convention the ijk indices correspond to the generations of the superfields \tilde{L}_i , \tilde{Q}_j and D_k containing respectively the left-handed lepton doublet, quark doublet and the right handed quark singlet. Expanded in terms of matter fields, the interaction Lagrangian reads [2]:

$$\begin{aligned} \mathcal{L}_{\tilde{L}_i \tilde{Q}_j D_k} = & \kappa_{ijk}^0 \left(\tilde{e}_L^i u_L^j d_R^k - \tilde{e}_L^i \nu_L^j d_R^k - (\tilde{e}_L^i)^c u_L^j d_R^k \right. \\ & \left. + \tilde{\nu}_L^i d_L^j d_R^k + \tilde{\nu}_L^i d_L^j d_R^k + (\tilde{\nu}_L^i)^c d_L^j d_R^k \right) + \text{h.c.} \end{aligned}$$

where the superscripts c denote the charge conjugate spinors and the $\tilde{}$ the complex conjugate of scalar fields. For the scalars the R' and L' indices distinguish independent fields describing superpartners of right- and left-handed fermions. Hence, with an e^+ in the initial state, the couplings κ_{ijk}^0 allow for resonant production of squarks through positron-quark fusion. The list of possible single production processes is given in table 1. In this paper, the squark search is carried with the simplifying assumptions that:

only one of the κ_{ijk}^0 dominates;

squarks (\tilde{q} and \tilde{q}_L) of the first and second generation are quasi-degenerate in mass (the case of the stop squark is considered separately);

the lightest supersymmetric particle is the lightest neutralino $\tilde{\chi}_1^0$;

Table 1: Squark production processes at HERA (e^+ beam) via a R-parity violating \tilde{g}_{1jk}^0 coupling.

\tilde{g}_{1jk}^0	production process	
111	$e^+ + u \rightarrow \tilde{d}_R$	$e^+ + d \rightarrow \tilde{\nu}_L$
112	$e^+ + u \rightarrow \tilde{s}_R$	$e^+ + s \rightarrow \tilde{\nu}_L$
113	$e^+ + u \rightarrow \tilde{b}_R$	$e^+ + b \rightarrow \tilde{\nu}_L$
121	$e^+ + c \rightarrow \tilde{d}_R$	$e^+ + d \rightarrow \tilde{c}_L$
122	$e^+ + c \rightarrow \tilde{s}_R$	$e^+ + s \rightarrow \tilde{c}_L$
123	$e^+ + c \rightarrow \tilde{b}_R$	$e^+ + b \rightarrow \tilde{c}_L$
131	$e^+ + t \rightarrow \tilde{d}_R$	$e^+ + d \rightarrow \tilde{t}_L$
132	$e^+ + t \rightarrow \tilde{s}_R$	$e^+ + s \rightarrow \tilde{t}_L$
133	$e^+ + t \rightarrow \tilde{b}_R$	$e^+ + b \rightarrow \tilde{t}_L$

gluinos are heavier than the squarks such that decays $\tilde{g} \rightarrow q + \bar{g}$ are kinematically forbidden.

The squarks decay either via their Yukawa coupling into fermions, or via their gauge couplings into a quark and either a neutralino $\tilde{\chi}_i^0$ ($i = 1; 4$) or a chargino $\tilde{\chi}_j^\pm$ ($j = 1; 2$). The mass eigenstates $\tilde{\chi}_i^0$ and $\tilde{\chi}_j^\pm$ are mixed states of gauginos and higgsinos and are in general unstable. In contrast to the MSSM, this also holds in \mathbb{R}_p SUSY for the lightest supersymmetric particle (LSP) which decays via \tilde{g}_{1jk}^0 into a quark, an antiquark and a lepton [2].

Typical diagrams for the production of first generation squarks are shown in Fig. 1. By gauge symmetry only the \tilde{d}_R and $\tilde{\nu}_L$ are produced via the \tilde{g}_{1jk}^0 couplings. These have in general widely different allowed or dominant decay modes.

In cases where both production and decay occur through a \tilde{g}_{1jk}^0 coupling (e.g. Fig. 1a and c for $\tilde{g}_{111}^0 \neq 0$), the squarks behave as scalar leptoquarks [3, 4]. For $\tilde{g}_{111}^0 \neq 0$, the \tilde{d}_R resemble the S^0 leptoquark and decays in either $e^+ + u$ or $e^+ + d$ while the $\tilde{\nu}_L$ resemble the $S_{1=2}^0$ and only decays into $e^+ + d$. Hence, the final state signatures consist of a lepton and a jet and are, event-by-event, indistinguishable from the SM neutral (NC) and charged current (CC) deep inelastic scattering (DIS). The strategy is then to look for resonances in DIS-like events at high mass, exploiting the characteristic angular distribution of the decay products expected for a scalar particle.

In cases where the squark decay occurs through gauge couplings (e.g. Fig. 1b and d), one has to consider for the $\tilde{\nu}_L$ the processes $\tilde{\nu}_L \rightarrow u \tilde{\chi}_1^0$ or $d \tilde{\chi}_1^\pm$ while for the \tilde{d}_R only $\tilde{d}_R \rightarrow d \tilde{\chi}_1^0$ is allowed. This is because the $SU(2)_L$ symmetry which implies in the SM that the right handed fermions do not couple to the W boson also forbids a coupling of \tilde{d}_R to the W^- . Hence, the \tilde{d}_R can only weakly couple (in proportion to the d quark mass) to the $\tilde{\chi}_j^\pm$ through its higgsino component.

The possible decay modes of the chargino, when it is the lightest chargino $\tilde{\chi}_1^\pm$, are the gauge decays $\tilde{\chi}_1^+ \rightarrow \tilde{\chi}_1^0 l^+$ and $\tilde{\chi}_1^+ \rightarrow \tilde{\chi}_1^0 q \bar{q}$, and the \mathbb{R}_p decays $\tilde{\chi}_1^+ \rightarrow u d$ and $\tilde{\chi}_1^+ \rightarrow e^+ d \bar{d}$. The fate of the $\tilde{\chi}_1^0$ depends on its gaugino-higgsino composition. The

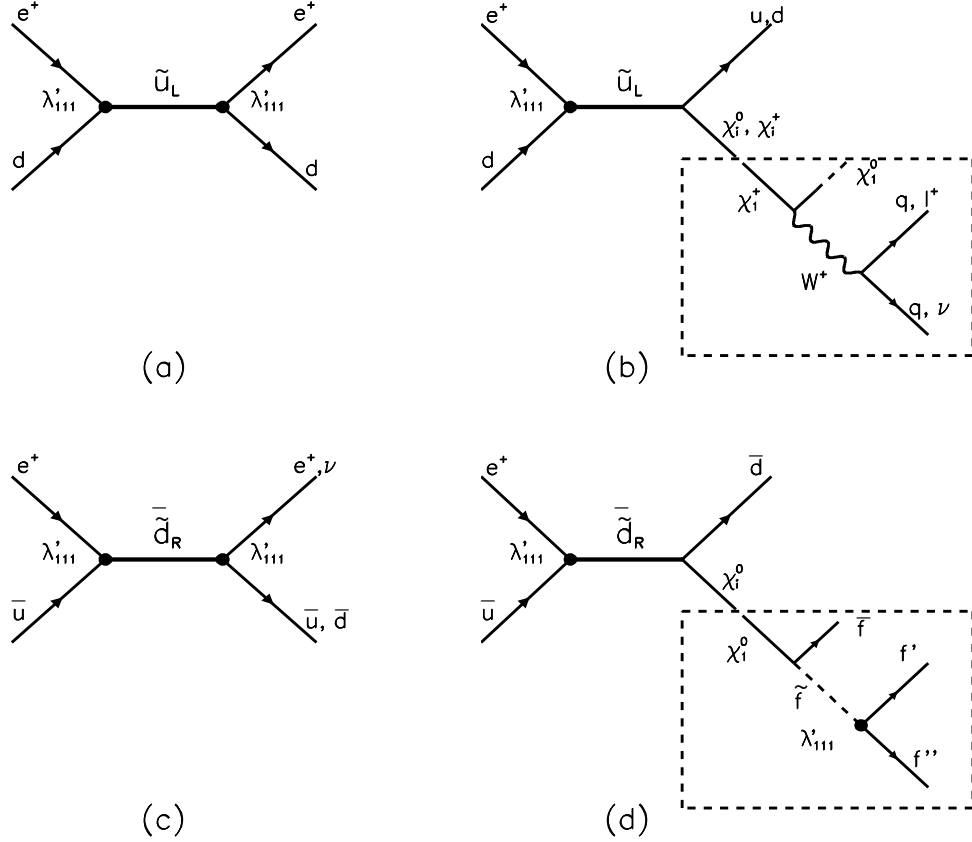


Figure 1: Lowest order s-channel diagrams for first generation squark production at HERA followed by (a),(c) \mathbb{B}_p decays and (b),(d) gauge decays. In (b) and (d), the emerging neutralino or chargino might subsequently undergo \mathbb{B}_p decays of which examples are shown in the dotted boxes for (b) the $\tilde{\chi}_1^0$ and (d) the $\tilde{\chi}_1^+$.

question of how this $\tilde{\chi}_1^0$ nature depends on free fundamental parameters of the MSSM, as well as the corresponding \mathbb{B}_p branching fractions for various possible decay channels will be discussed briefly in relation to our analysis in section 5 and was studied in more detail in [5, 6]. In general, the $\tilde{\chi}_1^0$ will undergo the decay $\tilde{\chi}_1^0 \rightarrow e^+ q \bar{q}$ or $\tilde{\chi}_1^0 \rightarrow q \bar{q}$. The former will be dominant if the $\tilde{\chi}_1^0$ is photino-like (i.e. dominated by photino components) in which case both the "right" and the "wrong" sign lepton (compared to incident beam) are equally probable leading to largely background free striking signatures for lepton number violation. The latter will dominate if the $\tilde{\chi}_1^0$ is zino-like. A higgsino-like $\tilde{\chi}_1^0$ will most probably be long lived and escape detection since its coupling to fermion-fermion pairs (e.g. Fig. 1d) is proportional to the fermion mass [7]. Hence processes involving a H-like $\tilde{\chi}_1^0$ will be affected by an imbalance in transverse momenta.

Taking into account the dependence on the nature of the $\tilde{\chi}_1^0$, the possible decay chains of the \tilde{u}_L and \tilde{d}_R squarks can be classified into eight distinguishable event topologies listed in tables 2 and 3 and labelled S1 to S8.

Channel	$\tilde{0}_1$ nature	Decay processes	Signature
S1	$\sim \tilde{Z}, \tilde{H}$	$\tilde{q} \rightarrow e^+ q^0$	High P_T e^+ + 1 jet
S2	$\sim \tilde{Z}, \tilde{H}, \tilde{H}^\pm$	$\tilde{q}_R \rightarrow e d$ $\tilde{q} \rightarrow q \tilde{0}_1$	Missing P_T + 1 jet
S3	$\sim \tilde{Z}$	$\tilde{q} \rightarrow q \tilde{0}_1$	High P_T e^+ + multiple jets
	$\sim \tilde{Z}, \tilde{H}$	$\tilde{u}_L \rightarrow d \tilde{0}_1$ $\tilde{d} \rightarrow u \tilde{0}_1$	
	$\sim \tilde{Z}$	$\tilde{u}_L \rightarrow d \tilde{0}_1$ $\tilde{d} \rightarrow u \tilde{0}_1$ $\tilde{q} \rightarrow W^+ q^0$ $\tilde{q} \rightarrow e^+ q^0 q^0$ $\tilde{q} \rightarrow q q^0$	
S4	$\sim \tilde{Z}$	$\tilde{q} \rightarrow q \tilde{0}_1$	High P_T e (i.e. wrong sign lepton) + multiple jets
	$\sim \tilde{Z}$	$\tilde{u}_L \rightarrow d \tilde{0}_1$ $\tilde{d} \rightarrow u \tilde{0}_1$ $\tilde{q} \rightarrow W^+ q^0$ $\tilde{q} \rightarrow e^+ q^0 q^0$ $\tilde{q} \rightarrow q q^0$	

Table 2: Squark decay channels in \mathbb{R}_p SUSY classified per distinguishable event topologies (first part). The dominant component of the $\tilde{0}_1$ for which a given decay chain is relevant is given in the second column. The list of processes contributing to a given event topology is here representative but not exhaustive, e.g. the gauge decays of the $\tilde{0}_1^+$ involving a virtual W^+ (Fig. 1b) may also proceed via a virtual fermion.

For a squark decaying into a quark and the lightest neutralino, the partial width can be written as

$$\Gamma(\tilde{q} \rightarrow q \tilde{0}_1) = \frac{1}{8} (A^2 + B^2) M_{\tilde{q}}^2 \left(1 - \frac{M_{\tilde{0}_1}^2}{M_{\tilde{q}}^2}\right)^2 \Rightarrow \Gamma(\tilde{q} \rightarrow q \tilde{0}_1) = \Gamma(\tilde{q} \rightarrow e q^0) \frac{2e^2 e_q^2}{g^2} \left(1 - \frac{M_{\tilde{0}_1}^2}{M_{\tilde{q}}^2}\right)^2$$

where A and B in the left expression are chiral couplings depending on the mixing parameters. Detailed expressions for such couplings can be found in [7]. Under the simplifying assumption that the neutralino is a pure photino $\tilde{\gamma}$, this gauge decay width reduces to the expression on the right. Here we introduced the partial width $\Gamma(\tilde{q} \rightarrow e q^0) = \frac{1}{8} M_{\tilde{q}}^2 = 16$ for squarks undergoing \mathbb{R}_p decays. It is seen that, in general, gauge decays contribute strongly at low $\tilde{0}_1$ masses and small Yukawa couplings.

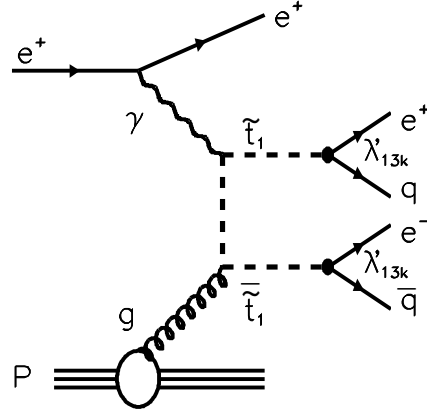
The case $\tilde{0}_{131} \notin 0$ (or $\tilde{0}_{132} \notin 0$) is of special interest [8] since it allows for direct production of the stop via $e^+ d \rightarrow \tilde{t}^* (e^+ s \rightarrow \tilde{t})$. The stop is particular in the sense that a "light" stop mass eigenstate (\tilde{t}_1) could (depending upon the mass parameters for the chiral states and on the free parameters of the model) exist much lighter than the top

Channel	$\tilde{0}_1$ nature	Decay processes	Signature
S5	$\sim \tilde{Z}$ $\sim \tilde{Z}$ $\sim \tilde{Z}, H$ H	$\tilde{q} \rightarrow q \tilde{0}_1$ $\tilde{u}_L \rightarrow d \tilde{0}_1$ $\tilde{u}_L \rightarrow d W^+ \tilde{0}_1$ $\tilde{u}_L \rightarrow d \tilde{q} \tilde{q}^0$ $\tilde{u}_L \rightarrow d u d$ $\tilde{u}_L \rightarrow d W^+ \tilde{q} \tilde{q}^0$	Missing P_T + multiple jets
S6	H	$\tilde{u}_L \rightarrow d \tilde{0}_1$ $\tilde{u}_L \rightarrow d W^+ \tilde{0}_1$ $\tilde{u}_L \rightarrow d I^+$	High P_T e^+ or μ^+ + missing P_T + 1 jet
S7	$\sim \tilde{Z}$	$\tilde{u}_L \rightarrow d \tilde{0}_1$ $\tilde{u}_L \rightarrow d W^+ \tilde{0}_1$ $\tilde{u}_L \rightarrow d \tilde{e} \tilde{q} \tilde{q}^0$ $\tilde{u}_L \rightarrow d I^+$	High P_T e + high P_T e^+ or μ^+ + missing P_T + multiple jets
S8	$\sim \tilde{Z}$	$\tilde{u}_L \rightarrow d \tilde{0}_1$ $\tilde{u}_L \rightarrow d W^+ \tilde{0}_1$ $\tilde{u}_L \rightarrow d \tilde{q} \tilde{q}^0$ $\tilde{u}_L \rightarrow d I^+$	High P_T e^+ or μ^+ + missing P_T + multiple jets

Table 3: Squark decay channels in \mathbb{R}_p SUSY classified per distinguishable event topologies (second part). As in table 2, the list of processes given here is not exhaustive, e.g. the gauge decays $\tilde{1}^+ \rightarrow \tilde{1}^+ \tilde{0}_1$ and $\tilde{1}^+ \rightarrow \tilde{1}^0 \tilde{q} \tilde{q}^0$ may also proceed via a virtual fermion.

quark itself and lighter than other squarks. This applies only for the stop since the off-diagonal terms which appear in the mass matrix associated to the superpartners of chiral fermions are proportional to the partner fermion mass. Such a stop \tilde{t}_1 mass eigenstate is considered in this paper and its search is furthermore extended towards low mass by considering pair production via γ -gluon fusion as illustrated in Fig. 2. For the study of this process, we assume that the \tilde{t}_1 is lighter than the lightest chargino. Hence the \tilde{t}_1 will decay dominantly into a positron and a quark since, by assumption, the decays into $\tilde{t} \tilde{0}_1$ and $b \tilde{1}^+$ are forbidden and the one-loop decay into $c \tilde{0}_1$ is negligible even for small values of the \mathbb{R}_p coupling of the \tilde{t}_1 to a positron-quark pair [5].

Figure 2: Stop pair production via γ -gluon fusion at HERA, followed by \tilde{t}_1 decay of the \tilde{t}_1 .



3 The H1 detector

A detailed description of the H1 detector can be found in [9]. Here we describe only the components relevant for the present analysis in which the event final state involves either an e^+ (or e^-) with high transverse energy or a large amount of hadronic transverse energy flow.

The e^+ (or e^-) energy and angle are measured in a finely segmented liquid argon (LAR) sampling calorimeter [10] covering the polar angle¹ range 4° – 153° and all azimuthal angles. It consists of a lead/argon electromagnetic section followed by a stainless-steel/argon hadronic section. Electromagnetic energies are measured with a resolution of $(E)/E = 12\%/\sqrt{E}$ and hadronic energies with $(E)/E = 50\%/\sqrt{E}$ after software energy weighting [11]. The absolute scales are known to 2% and 5% for electromagnetic and hadronic energies respectively. The angular resolution on the scattered electron measured from the electromagnetic shower in the calorimeter is ~ 4 mrad. A lead/scintillator electromagnetic backward calorimeter extends the coverage at larger angles (155° – 176°).

Located inside the calorimeters is the tracking system used here to determine the interaction vertex and the charge of the final state lepton. The main components of this system are central drift and proportional chambers (25–155), a forward track detector (7–25) and backward proportional chambers (155–175). The tracking chambers and calorimeters are surrounded by a superconducting solenoid coil providing a uniform field of 1.15 T within the tracking volume. The instrumented iron return yoke surrounding this coil is used to measure leakage of hadronic showers and to recognize muons. The luminosity is determined from the rate of the Bethe-Heitler process $ep \rightarrow e\gamma p$ measured in a luminosity monitor.

¹The incoming proton moves by definition in the forward ($z > 0$) direction with $\theta = 0^\circ$ polar angle.

4 Analysis

4.1 Single production of squarks

For the search for resonant production of squarks, the event selection basically relies on the final state lepton finding and on global energy-momentum conservation cuts. It is optimized separately for each of the event topologies (see tables 2 and 3) S1 to S8 by relying on Monte Carlo simulation.

The simulation of the leptoquark-like signatures (S1 and S2) relies on the event generator LEGO [12]. For squarks undergoing gauge decays followed by a $\frac{0}{1}$ or $\frac{+}{1} \mathbb{K}_p$ decay into a high P_T lepton and multiple jets, i.e. processes belonging to topologies S3 and S4, the generator SUSSEX [12] based on the cross-sections given in [2] is used. Both generators also simulate initial state bremsstrahlung in the collinear approximation, initial and final state parton showers and fragmentation [13, 14], and properly take into account the correction of the kinematics at the decay vertex for effects of the parton shower masses. The parton densities used [15, 16] are evaluated at the scale of the new particle mass, and this scale is also chosen for the maximum virtuality of parton showers. For these channels, a complete simulation of the H1 detector response is performed. The event topologies S5 to S8 (as well as some of the processes in S3 or S4 which proceed through the exchange of a virtual W or virtual sfermion), were studied at four-vector level [6] taking into account matrix element calculations [18] and multiparticle phase space. For these channels, realistic efficiencies are then obtained by smearing the particle four-vectors according to measured resolutions, detector effects and acceptances. The efficiencies thus obtained were cross-checked and found to agree typically within 5% with a complete simulation based on SUSSEX for those S5 processes where the $\frac{+}{1}$ undergoes a \mathbb{K}_p violating decay.

A complete Monte Carlo simulation of the H1 detector response is performed for each possible background source. For the DIS NC or CC background estimates we make use of either the DJANGO [19] or the LEPTO [20] event generator. DJANGO includes first order radiative corrections and simulation of real bremsstrahlung photons based on HERACLES [21], as well as QCD dipole parton showers based on ARIADNE [22]. LEPTO includes the lowest order electroweak scattering process with QCD corrections to first order in α_s , complemented by leading-log parton showers and string fragmentation [23]. Both generators agree in channels where one expects a single hard jet, i.e. S1, S2 and S6. The LEPTO event generator is used in the multijet channels S3, S4, S5, S7 and S8.

The parton densities in the proton used for DIS throughout are taken from the MRS H [16] parametrization which is close to F_2 structure function measurements at HERA (see [24]). For the direct and resolved photoproduction of light and heavy flavours, the PYTHIA MC event generator [13] is used which includes QCD corrections to first order in α_s , leading-log parton showers and string fragmentation [14]. The GRV LO (GRV-G LO) parton densities [25] in the proton (photon) are used at low Q^2 .

The event selection for real data starts with the rejection of non-colliding background. This selection step is common to all channels and requires:

1. a primary interaction vertex in the range $|z - z_0| < 35$ cm with $z_0 = 3.4$ cm;
2. that the event survives a set of halo and cosmic muon filters; for channel S2 these are complemented by visual scan;
3. that the event be properly in time relative to interacting bunch crossings.

Cut (1) mainly suppresses beam {wall, beam {residual gas and, with (2) and (3), background from cosmic rays and halo muons. We moreover impose that the events be accepted by LAr calorimetry triggers [10]: the events of S1, S3 and S4 must satisfy "\electron" or "\transverse energy" trigger requirements; events of S2 and S5 must fulfill "\missing transverse energy" requirements; events of S6, S7 and S8 must satisfy either "\electron" or "\missing transverse energy" requirements.

The selection cuts and data reduction specific to each of the event topologies for the ep-induced background is presented below. In each case the number of event candidates observed are compared to SM expectations. The systematic (syst.) errors quoted on the mean expected background in each case take into account uncertainties on the absolute electromagnetic and hadronic energy scales (see section 3), on the integrated luminosity (1.5%) and the contribution due to finite Monte Carlo statistics. Estimates of SUSY signal detection efficiencies are also given in each channel.

Event topology S1:

For the event topology S1, i.e. events characterized by the DIS NC-like signatures [3], it is necessary to reject contaminating background from other physical processes. We require:

1. an isolated e^+ cluster [26] with $E_{T,e} = E_e \sin \theta_e > 7$ GeV and $10^\circ < \theta_e < 145^\circ$; (here e^+ includes all candidates except those having an associated track with explicitly measured negative charge); the isolation requires that less than 10% additional energy be found within a pseudorapidity-azimuth cone of opening $(\Delta \eta)^2 + (\Delta \phi)^2 < 0.25$ centered on the e^+ candidate;
2. that if two e^+ cluster candidates are found, they must not be balanced in $E_{T,e}$ and in azimuth, i.e. $E_{T,e}^1 = E_{T,e}^2 > 1.25$ and $|j_{1,2} - 180| \geq 2^\circ$, and the candidate with highest $E_{T,e}$ must be at smallest rapidity;
3. a total missing transverse momentum $P_{T,miss} = \sqrt{\sum_i (E_x^i)^2 + \sum_i (E_y^i)^2} > 15$ GeV summed over all energy depositions i in the calorimeters, with $E_x^i = E^i \sin \theta^i \cos \phi^i$ and $E_y^i = E^i \sin \theta^i \sin \phi^i$;
4. a minimal "\longitudinal momentum" loss in the direction of the incident positron, $8 - 2E_e^0 (E - P_z) > 12$ GeV, where E_e^0 is the incident positron beam energy;
5. a y_e , measured from the final state e^+ , satisfying $y_e < 0.95$.

Cuts (1) and (3) eliminate DIS CC events. Cut (2) suppresses QED Compton events. Cut (4) provides a powerful rejection of photoproduction contamination and also suppresses DIS NC-like events with a very hard γ emitted from the initial state positron. Cut (5) further suppresses photoproduction with a "fake" e which tends to cluster at largest y_e for largest M_e , where y_e is the standard DIS Lorentz invariant and M_e the "squark mass" reconstructed from the final state e^+ energy E_e and angle θ_e as :

$$M_e = \sqrt{s} \frac{Q_e^2}{y_e} = \frac{Q_e^2}{y_e}; \quad Q_e^2 = \frac{E_{T,e}^2}{1 - y_e}; \quad y_e = 1 - \frac{E_e - E_e \cos \theta_e}{2E_e^0};$$

Q^2 is the standard momentum transfer squared of DIS. In addition to the above requirements, we apply a M_e dependent y_e cut which is designed [1, 3] via Monte Carlo studies to optimize the signal significance for scalar leptoquark searches, given the expected background. This y_e cut varies from $y_e > 0.5$ at 45 GeV to $y_e > 0.35$ at 150 GeV and down to $y_e > 0.05$ at 275 GeV.

For these NC-like (leptoquark like) signatures, 362 events satisfy the selection requirements and the y_e cut in the mass range $M_e > 25$ GeV. This observed number of events is in good agreement with the mean expected DIS NC background of 335 ± 36 (syst.) events. The measured mass spectrum is compared to the DIS NC expectation in Fig. 3. For $M_e > 45$ GeV, we are left with 91 events while 84 ± 10.2 (syst.) events are expected

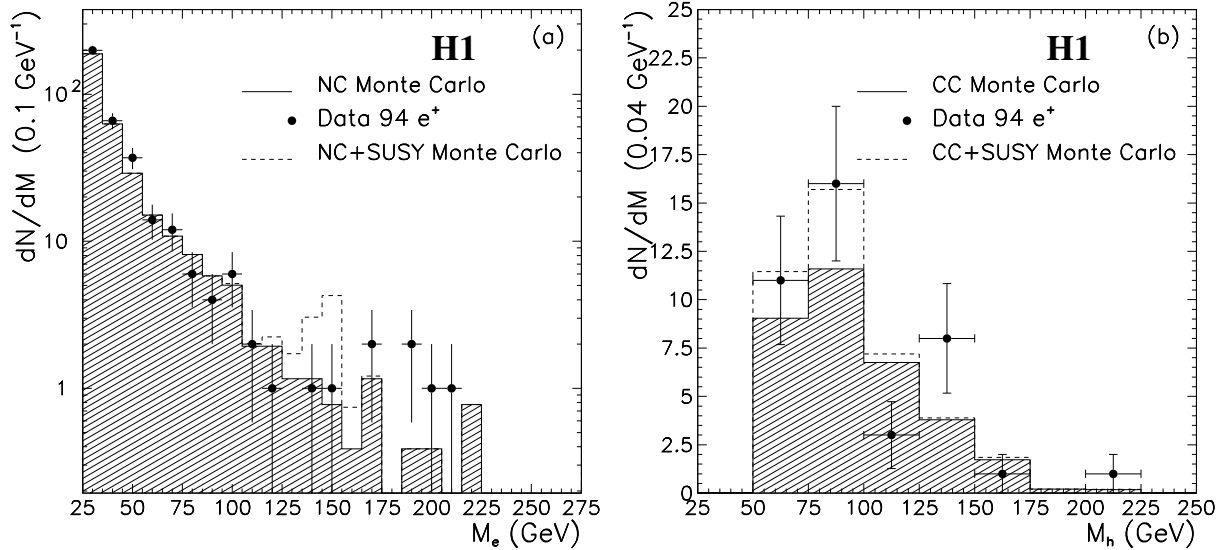


Figure 3: Mass spectra for (a) $e + q$ (b) $e + q$ final states for data (closed points) and DIS Monte Carlo (shaded histograms). The superimposed dashed histograms show typical \tilde{K}_p SUSY signals near the sensitivity limit (see table 4 in section 5) for (a) $M_q = 150$ GeV and $M_{\tilde{g}} = 20$ GeV and for (b) $M_q = 75$ GeV and $M_{\tilde{g}} = 20$ GeV.

from the SM. For $M_e > 100$ GeV, 13 events are observed in good agreement with the mean SM expectation of 12.4 ± 2.6 (syst.).

In this channel, the \mathbb{E}_p SUSY signal detection efficiency is found to be weakly dependent on $M_{\tilde{q}}$ and ranges from 43% at 45 GeV to 68% at 150 GeV in the middle of the mass range considered here.

Event topology S2:

The event topology S2 is characterized by DIS CC-like signatures [3] for which we require:

1. no electron cluster satisfying the above S1 requirements;
2. $P_{T,miss} > 25 \text{ GeV}$;
3. the total transverse energy $E_T^P = \sum_j P_T^j$ calculated from energy depositions in the calorimeter should match the total missing transverse momentum $P_{T,miss}$ such that $(E_T - P_{T,miss})/E_T < 0.5$.

Cuts (1) to (3) eliminate photoproduction and DIS NC background.

In total, 40 CC-like events satisfy all above requirements in the relevant mass and y range at $M_h > 45 \text{ GeV}$ and $y_h < 0.95$ where M_h and y_h are reconstructed by summing over all measured final state hadronic energy:

$$M_h = \sqrt{\sum_h^2 \frac{Q_h^2}{Y_h}}; \quad Q_h^2 = \frac{P_{T,miss}^2}{1 - Y_h}; \quad Y_h = \frac{P_z}{2E_e^0}.$$

As is seen in Fig. 3b, this is in good agreement with the DIS CC expectation of 33.4 ± 3.6 (syst.) events.

The \mathbb{E}_p SUSY signal detection efficiency in this channel rises from 15% at 45 GeV to reach a plateau at 80% above 100 GeV.

Event topology S3:

For a gauge decay of the squarks leading to a "right" signal state lepton (i.e. $e^+ q \rightarrow q + \tilde{q}_1^0 + q^0 \rightarrow e^+ q \tilde{q}^0 \tilde{q}^0$), we impose the following stringent requirements in complement to S1 cuts:

1. the e^+ must give $y_e > 0.4$;
2. an imbalance between the total hadronic $E_{T,h}$ and $P_{T,h}$ such that $(E_{T,h} - P_{T,h})/E_{T,h} > 0.25$;
3. at least one reconstructed jet with $P_{T,jet} > 7 \text{ GeV}$;
4. the azimuthal opening angle θ_{jet} between the jet of highest P_T (i.e. generally the current jet in a DIS NC process) and the axis defined by the total hadronic transverse momentum $\vec{P}_{T,h} = (\sum_h E_{x,h}; \sum_h E_{y,h})$ be larger than $\theta_{jet} > 2.5 \text{ rad} \text{ (} 50^\circ \text{)}$ with $E_{T,h}$ in GeV and θ_{jet} in degrees;

5. the squark invariant mass calculated from all final state particles (M_{dec}) excluding the proton fragments [1] must deviate from $M_{\tilde{q}}$ by more than 10%.

Cut (1) strongly suppresses DIS NC background. The y_e distribution calculated from the \tilde{e}^+ in SUSY events appears strongly shifted towards large y_e since the squark decays uniformly in its center-of-mass frame and, further, since the \tilde{e}^+ takes away only a fraction of the $\frac{0}{1}$ momentum. Cut (2) exploits the fact that the hadronic energy of the event is not concentrated within one single jet because of the decay products of the $\frac{0}{1}$. Fig. 4a shows how this value discriminates the DIS NC background from the signal. The jet finding for cuts (3) and (4) relies (here and throughout the paper) on a simple cone algorithm in the laboratory reference frame with a fixed pseudorapidity-azimuth opening radius of 1 unit. Cut (4) further suppresses lowest order DIS NC events by imposing sufficient hadronic activity far enough in azimuth from the "current" jet. Cut (5) ensures that the events accepted here (gauge decay modes) are not simultaneously accepted as S1 candidates (\tilde{g}_p decay modes).

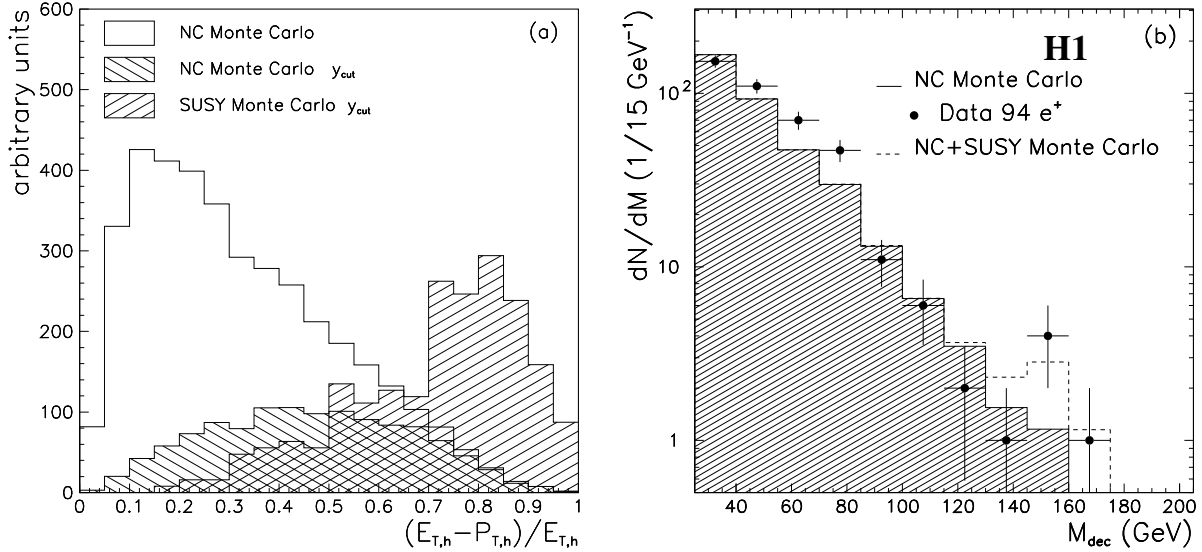


Figure 4: (a) Balance between the total scalar hadronic energy $E_{T,h}$ and the vector sum $P_{T,h}$ for DIS NC before and after the $y_e > 0.4$ cut and for a simulation of a 150 GeV squark decaying into $e^+ q \tilde{e}^+ q^0 q^0 q^0$; (b) measured mass spectrum (uncorrected) for the squark candidates in the $e^+ q \tilde{e}^+ q^0 q^0 q^0$ channel for data (dots) and DIS NC Monte Carlo (histogram), the superimposed dashed histogram in (b) show a typical \tilde{g}_p SUSY signal near the sensitivity limit (see table 4 in section 5) for $M_{\tilde{q}} = 150$ GeV and $M_{\tilde{e}} = 40$ GeV.

We find 405 candidates satisfying the previous cuts for masses $M_{\text{dec}} > 25$ GeV, which is to be compared with the mean SM background of 363 ± 39 events expected from DIS NC. The measured mass spectrum is compared to Monte Carlo expectations in Fig. 4b. Above 45 GeV we observe 220 events in the data, while 154 ± 17 (syst.) events are expected

from DIS NC. This represents an excess of 2.9 standard deviations in the Gaussian limit approximation (combining statistical and systematic errors in quadrature). The slight excess of events is seen to be mostly concentrated at low masses and in particular in the mass range from 40 to 85 GeV. Nevertheless, it should be recalled here that our DIS NC Monte Carlo for multijet channels (LEPTO) does not include full QED corrections which could lead to a migration of events with true y_e below cut (1) towards larger apparent y_e . A good agreement is observed for $M_{dec} > 100$ GeV where we find 14 events while the mean DIS NC expectation is 13.2 ± 2.6 (syst.) events. For $M_{dec} > 140$ GeV, 5 events are found which agrees well with the expectation of 1.9 ± 0.9 (syst.).

In this channel, the \mathbb{R}_p SUSY signal detection efficiencies (which experimentally sum to that of both the right sign and the unsigned events), depend mainly on the η_1^0 . For $M_{\eta_1^0} = 20$ GeV it rises from 20% for $M_{\eta} = 45$ GeV to a plateau of 33% for $M_{\eta} \geq 75$ GeV. For $M_{\eta_1^0} = 80$ GeV it reaches 60% for $M_{\eta} \geq 100$ GeV.

Event topology S4:

For a gauge decay of the squarks leading to a "wrong" signal state lepton (i.e. $e^+ q \rightarrow \bar{q} \rightarrow e^- q \bar{q} q \bar{q}$) we perform a determination of the lepton charge using the tracking chamber information. Hence, we impose in addition to the above S3 criteria :

1. the electron cluster must be geometrically linked to a negatively charged track and the cluster energy must match the track momentum within $j(E - P) = (E + P) < 0.5$;
2. the track must be made of at least 40 digitisations in the central tracking chamber;
3. the error in the curvature must fulfil $\Delta j = \Delta j > 1$.

These cuts ensure a good quality of the track reconstruction and track-cluster matching at the expense of a reduced efficiency (partly due to occasional inoperation of either the inner or the outer central drift chambers) for accepting the electron track of about 70% in the angular range 35° well covered by the central tracking chambers.

We observe no electron (wrong sign) events among the 405 candidates satisfying the kinematical requirements for squark gauge decays.

In this channel, the charge track requirements imply an additional efficiency loss compared to S3 for the \mathbb{R}_p SUSY signal which is negligible at 45 GeV but which increases to 10% at 150 GeV and 20% at 250 GeV.

Event topology S5:

The event topology S5 is characterized by large missing transverse momentum and multiple jets. We require:

1. no electron cluster satisfying the above S1 requirements;
2. $P_{T,miss} > 15$ GeV;

3. $(E_{T,ph} - P_{T,ph}) = E_{T,ph} > 0.25;$
4. $P_{T,ph} > 50 \quad (1 - (E_{T,ph} - P_{T,ph}) = E_{T,ph})$ with $P_{T,ph}$ in GeV;
5. at least one reconstructed jet with $P_{T,jet} > 7 \text{ GeV}$; the jet of highest P_T should satisfy $\eta_{jt} > (4=7) \quad (100 - E_{T,ph})$ with η_{jt} in degrees and $E_{T,ph}$ in GeV.

Cut (3) exploits the fact that more than one jet is expected in such events. Cut (4) removes the DIS CC background, which is mainly concentrated at low values of $(E_{T,ph} - P_{T,ph}) = E_{T,ph}$. Cut (5) removes photoproduction events for which one of the two back-to-back jets is badly measured, so that the η_{jt} is expected to be small. We are left with 9 events in the data sample compared to an expectation of 3.9 ± 4 (syst.) events from p photoproduction background and a negligible DIS CC background. Here a sizeable contribution to the systematic error originates from the dependence of the LAr trigger efficiency on this S5 multijet topology.

It is shown in Fig. 5 how these 9 remaining events compare to the SM photoproduction and DIS CC expectations (respectively for $1 \cdot L_{data}$ and $10 \cdot L_{data}$). No LAr trigger efficiency losses are folded in the Monte Carlo sample of Figs. 5b,c, and d. It can be seen also that cut (5) still ensures a good efficiency for a possible SUSY signal.

The efficiency for \mathbb{K}_p SUSY events in S5 rises with increasing $M_{\tilde{q}}$ up to a plateau for $M_{\tilde{q}} \gtrsim 150 \text{ GeV}$. It also rises with increasing $M_{\tilde{0}_1}$ mainly because of the $P_{T,miss}$ selection cut imposed. For processes where the final state $\tilde{0}_1$ (or $\tilde{+}_1$) at the squark decay vertex directly undergoes a \mathbb{K}_p decay, the efficiency at $M_{\tilde{q}} \gtrsim 150 \text{ GeV}$ is 26% for $M_{\tilde{0}_1} = 20 \text{ GeV}$ and 52% for $M_{\tilde{0}_1} = 80 \text{ GeV}$. When the $\tilde{0}_1$ is H^\pm -like (stable) the mass difference between the $\tilde{0}_1$ and the $\tilde{+}_1$ is relatively smaller for heavier $\tilde{0}_1$ and this hampers the signal detection. Hence in processes where the $\tilde{0}_1$ escapes detection, the efficiency which at $M_{\tilde{q}} \gtrsim 150 \text{ GeV}$ reaches 50% for $M_{\tilde{0}_1} = 20 \text{ GeV}$ is down to 30% for $M_{\tilde{0}_1} = 80 \text{ GeV}$. Finally, processes where the $\tilde{+}_1$ undergoes a cascade decay (e.g. $\tilde{+}_1 \rightarrow W^+ \tilde{0}_1$; $\tilde{0}_1 \rightarrow e^+ q \bar{q} \bar{q}^0$; $W^+ \rightarrow q \bar{q}^0$), suffers from an efficiency loss due to the $P_{T,miss}$ cut. In such case the efficiency rises from 6% at $M_{\tilde{q}} = 100 \text{ GeV}$ to 32% at $M_{\tilde{q}} = 175 \text{ GeV}$.

Event topology S6:

The event topology S6 is characterized by the presence of a lepton (e^+ or μ^+) at large transverse energy $E_{T,l}$, a large missing transverse momentum and a single jet.

To search for cases where the final state lepton is a positron, we require:

1. an isolated e^+ with $E_{T,e} > 7 \text{ GeV}$;
2. $P_{T,miss} > 15 \text{ GeV}$;
3. $(E_{T,ph} - P_{T,ph}) = E_{T,ph} < 0.5;$
4. $0.4 < y_e < 0.95;$
5. at least one reconstructed jet with $P_{T,jet} > 7 \text{ GeV}$;

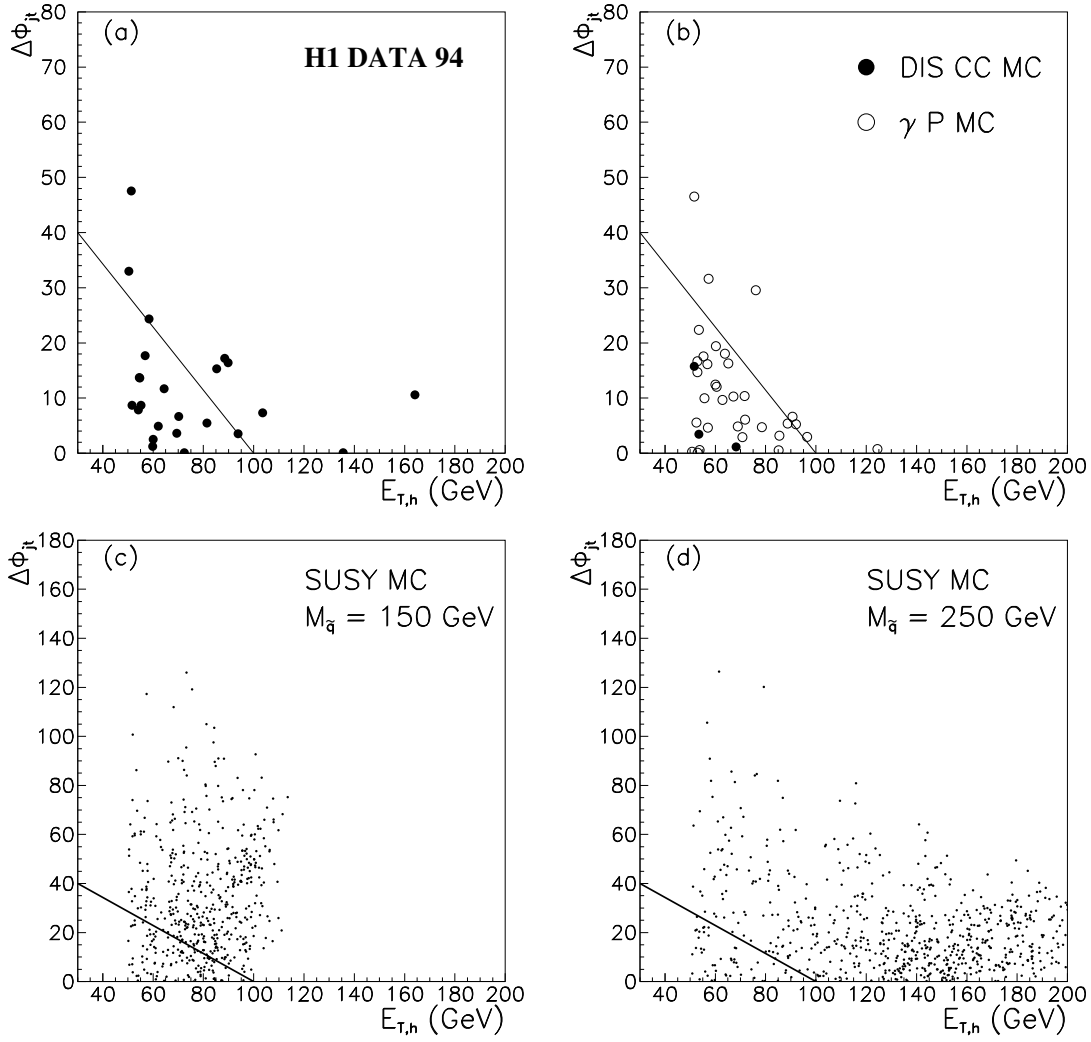


Figure 5: Correlation between the azimuthal opening angle $\Delta\phi_{\pi}$ and the total hadronic transverse energy $E_{T,h}$ for (a) data, (b) DIS CC and γp background MC and (c), (d) \tilde{E}_p SUSY signal in topology S5 for two example cases. The events above the cut (solid line) are accepted.

6. at least 1 charged track with $P_{\text{track}} > 5 \text{ GeV}$ originating from the primary vertex and linked to the electron cluster.

Cut (1) suppresses DIS CC background while cut (2) suppresses photoproduction background. The other cuts are designed to optimize the specific S6 signal significance relative to tails of background distributions. We are left with 2 event candidates in the data while 3.8 ± 1.3 (syst.) are expected from DIS NC background.

To search for cases where the final state lepton is a muon, we require:

1. no isolated e^- with $E_{T,e} > 7 \text{ GeV}$;
2. $P_{T,\text{miss}} > 25 \text{ GeV}$ calculated from the energy depositions in the calorimeters;
3. $(E_{T,h} - P_{T,h}) = E_{T,h} < 0.5$;

4. at least one reconstructed jet with $P_{T,jet} > 7 \text{ GeV}$;
5. at least 1 charged track with $P_{track} > 10 \text{ GeV}$ linked to the primary vertex and lying outside of a $\Delta\theta = 60^\circ$ cone centered on the direction of the jet at highest $P_{T,jet}$;
6. that the charged track in cut (5) be "penetrating" in the sense that there be $< 5 \text{ GeV}$ of total energy measured in the LAr calorimeter within a $\Delta\theta = 15^\circ$ cone centered on the track direction; moreover the track should not point to a cluster localized around the azimuthal cracks in the LAr calorimeter.

We are left with 1 event candidate in the data of which an event display is shown Fig. 6. A remarkable " $e^+ + \text{jet}$ " signature is seen (Fig. 6a) with a positively charged isolated track. A detailed analysis of this event [27] reveals that the isolated track has a transverse

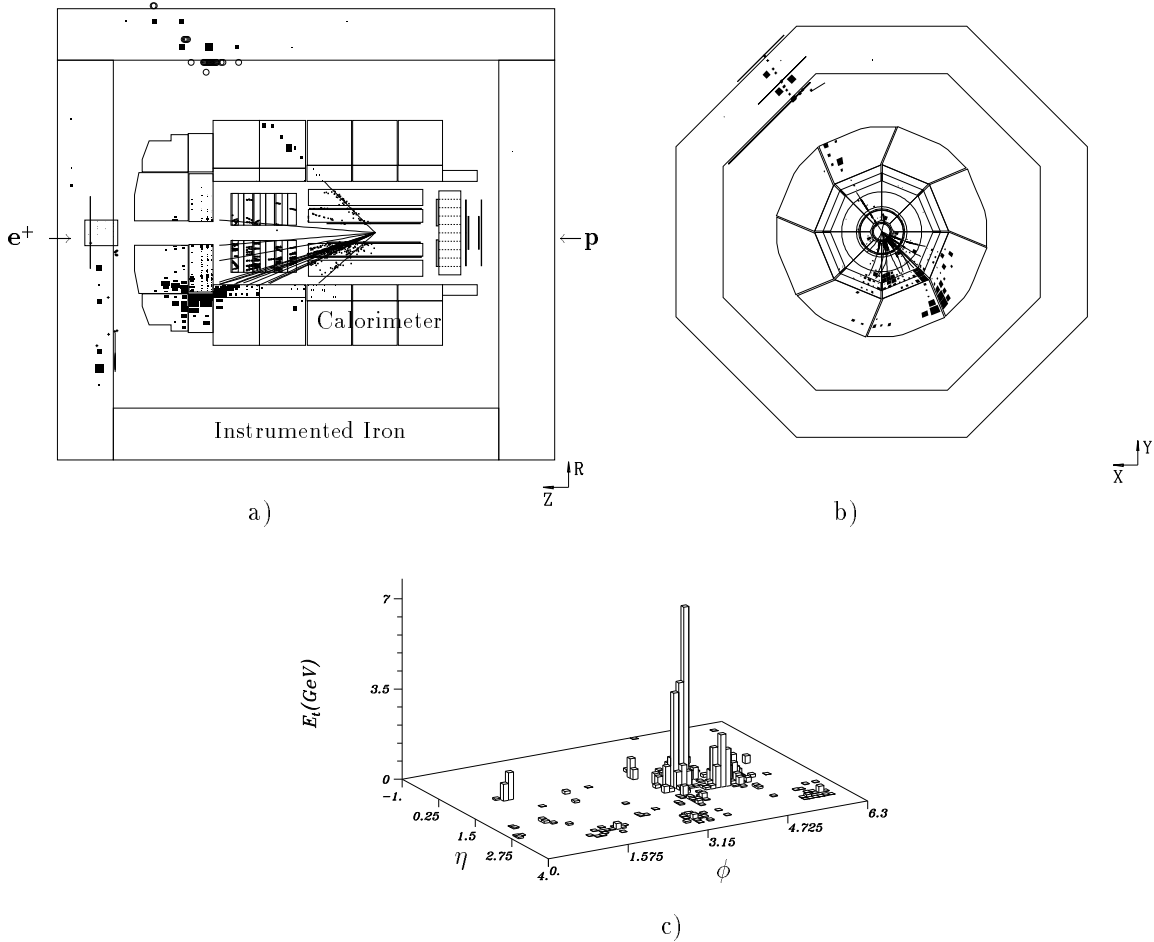


Figure 6: Display of the $e^+ p \rightarrow e^+ + \text{jet}$ candidate from H1 run number 84295 showing (a) an R-z view, (b) an R- ϕ view and (c) the calorimetric transverse energy flow.

momentum of $23.4^{+7.5}_{-5.7} \text{ GeV}$ and appears in azimuth at $\phi_{jet} = 183^\circ \pm 1^\circ$ from an hadronic system (Fig. 6b) which itself has in total $P_{T,h} = 42.1 \pm 4.2 \text{ GeV}$. This hadronic system is built from two main "clusters" (Fig. 6c) which are found to be merged into a

single jet with our cone algorithm within a radius of 1 unit in the pseudorapidity-azimuth plane. This leaves overall a total missing transverse momentum of $j \vec{P}_{T,ph} + \vec{P}_T$; $j = 18.7 \pm 4.8^{+5}_{-6}$ GeV and a longitudinal momentum loss in the incident positron direction of $2E_e^0 - f^p(E_h - P_{z,ph}) + (E - P_{z,j})g = 35.8 \pm 1.6^{+3}_{-2.1}$ GeV.

With our selection cuts (1) – (6), we expect on average from DIS CC a background of 0.04 ± 0.03 (syst.) event corresponding to a probability of about 4% to observe here one or more such event. The actual dominating background is expected [27] to come from associated W^+ production in NC and CC processes followed by a leptonic decay of the W^+ , $e^+p \rightarrow e^+W^+X \rightarrow e^+ + X$, where the final state e^+ is lost in the beam pipe. With our selection cuts, this process studied in a Monte Carlo calculation using the SM cross-section of [28] gives a 15% probability for such a background event to be accepted.

The efficiency for \mathbb{B}_p SUSY events in S6 rises with increasing $M_{\tilde{q}}$ up to a plateau for $M_{\tilde{q}} \gtrsim 150$ GeV, and decreases with increasing $M_{\tilde{g}}$ for reasons already explained in topology S5 for H^\pm -like \tilde{g}_1 . For $M_{\tilde{q}} \gtrsim 150$ GeV it is of 50% for $M_{\tilde{g}} = 20$ GeV, and down to 35% for $M_{\tilde{g}} = 80$ GeV.

It is interesting to note [29] that an \mathbb{B}_p SUSY signal is consistent with the properties of the observed event candidate. Imposing more restrictive requirements such as: $2E_e^0 - f^p(E_h - P_{z,ph}) + (E - P_{z,j})g > 12$ GeV, $p_{T,ph} > 140$, $P_{T,ph} > 40$ GeV and $P_{T,j} > 10$ GeV, we find that more than 30% of the \mathbb{B}_p SUSY events satisfying the selection cuts (1) to (6) in the muon channel also verify these additional requirements provided that the \tilde{u}_L be in the mass range $100 \leq M_{\tilde{u}_L} \leq 200$ GeV and the \tilde{t}_1 be in the range $20 \leq M_{\tilde{t}_1} \leq 30$ GeV for $M_{\tilde{u}_L} \leq 100$ GeV or $20 \leq M_{\tilde{t}_1} \leq 110$ GeV for $M_{\tilde{u}_L} \geq 200$ GeV.

With the above stringent requirement that $P_{T,ph} > 40$ GeV applied on the background, which implies in associated W^+ production a very stiff recoiling hadronic system, one is left with a 3% probability for such interpretation of the event and a negligible contribution from misidentified DIS CC events.

Event topology S7:

The event topology S7 is characterized by the presence of an e^- at large E_T , accompanied by another lepton l^+ , large missing transverse momentum and multiple jets. We require:

1. an isolated e^- with $E_{T,e} > 7$ GeV and giving $0.4 < y_e < 0.95$;
2. $P_{T,miss} > 15$ GeV;
3. $(E_{T,ph} - P_{T,ph}) = E_{T,j} > 0.25$;
4. at least one reconstructed jet with $P_{T,jet} > 7$ GeV.

In the case where l^+ is a positron we require in addition a second isolated e^- with $E_T > 5$ GeV. We observe no candidate in the data while 0.4 ± 0.3 event is expected on average from DIS NC and none from DIS CC. In the case where l^+ is a muon we impose a more stringent cut on $P_{T,miss} > 25$ GeV. We observe no candidate in the data, while 0.4 ± 0.3 event is expected on average from DIS NC and none from DIS CC.

The efficiency for \mathbb{K}_p SUSY events in S7 depends weakly on $M_{\tilde{q}}$ and rises with $M_{\tilde{l}_1^0}$. It is of 20% for $M_{\tilde{l}_1^0} = 20$ GeV and rises in the case where l^+ is a positron to 60% for $M_{\tilde{l}_1^0} = 80$ GeV. In the case where l^+ is a muon and for heavy \tilde{l}_1^0 , the apparent $P_{T,miss}$ tends to be reduced by the quasi-collinearity of the \tilde{l}_1^0 and neutrino in the final state and the efficiency only reaches 30% for $M_{\tilde{l}_1^0} = 80$ GeV.

Event topology S8:

The event topology S8 is characterized by the presence of one charged lepton (e^+ or μ^+) at large E_T , a large missing transverse momentum and multiple jets.

For the case where the lepton is a positron, we require:

1. an isolated e^+ with $E_{T,e} > 7$ GeV and giving $0.4 < y_e < 0.95$;
2. $P_{T,miss} > 15$ GeV;
3. $(E_{T,h} - P_{T,h}) = E_{T,h} > 0.25$;
4. at least one reconstructed jet with $P_{T,jet} > 7$ GeV.

We are left with 3 candidates in the data while 2.3 ± 1.0 are expected from DIS NC. The background from DIS CC and photoproduction is here negligible.

For the case where the lepton is a muon, we require:

1. no isolated e with $E_{T,e} > 7$ GeV;
2. $P_{T,miss} > 25$ GeV;
3. $(E_{T,h} - P_{T,h}) = E_{T,h} > 0.25$;
4. at least one reconstructed jet with $P_{T,jet} > 7$ GeV;
5. at least 1 "penetrating" and isolated charged track with $P_{track} > 10$ GeV, such tracks were defined in cuts (5) and (6) of the S6 selection.

We are left in the data with the same $e^+ X$ event candidate as was found in S6 event topology while 0.04 ± 0.03 event is expected from DIS CC background.

The efficiency for \mathbb{K}_p SUSY events in S8 has similar $M_{\tilde{q}}$ and $M_{\tilde{l}_1^0}$ dependence as in S7. It is of 20–30% for $M_{\tilde{l}_1^0} = 20$ GeV and rises in the case where l^+ is a positron to 65% for $M_{\tilde{l}_1^0} = 80$ GeV. In the case where l^+ is a muon, it remains at 25% for $M_{\tilde{l}_1^0} = 80$ GeV.

While the efficiency is rather high for the \mathbb{K}_p SUSY signal to satisfy the basic cuts (1) to (5), it is here (contrary to the S6 channel) difficult to meet the more restrictive conditions [29] that could be imposed on the observed $e^+ X$ event candidate. In particular, the overlap of hadronic P_T flow initiated by the three quark jets into a single observed jet and with $p_h > 140$ is a unlikely configuration. It is moreover difficult to satisfy simultaneously the stringent cut $2E_e^0 - f^0 (E_h - P_{z,h}) + (E_e - P_{z,e})g > 12$ GeV. We find that less than 10% of the \mathbb{K}_p SUSY events satisfying the selection cuts (1) to (5) also verify these additional requirements for $\tilde{\nu}_L$ be in the mass range $100 < M_{\tilde{\nu}_L} < 200$ GeV.

4.2 Pair production of stop squarks

For squarks which are pair produced in $\gamma\gamma$ -gluon fusion processes (Fig. 2), the scattered electron is generally lost in the beam pipe. The optimization of the event selection relies on Monte Carlo simulation. The simulation of stop pair production in $\gamma\gamma$ -gluon fusion [6] is based on the σ_{stop} cross-section calculated in the Weizsacker-Williams approximation. The resolved photon contribution [34] as well as the contribution from a Z_0 boson exchange are neglected. The GRV LO gluon density in the proton [25] is used. The background simulation is based on the event generator DJANGO [19] for DIS NC and PYTHIA [13] for photoproduction processes. We impose:

1. $P_{T,\text{miss}} > 15 \text{ GeV}$;
2. two e^- candidates satisfying $E_{T,e}^i > 5 \text{ GeV}$ within $10 < q_e^i < 145$, the e^- must be isolated within pseudorapidity-azimuth cones of opening $\sqrt{(\Delta\eta_e^i)^2 + (\Delta\phi_e^i)^2} < R_i$ where $R_{i=1} = 0.5$ and $R_{i=2} = 0.25$;
3. the two e^- candidates must be acollinear in the transverse plane, $\phi_{1,2} < 140^\circ$;
4. there must be missing "longitudinal momenta" such that $2E_e^0 - P_z > 12 \text{ GeV}$;
5. at least two jets must be found by the jet cone algorithm each with $E_{T,\text{jet}} > 5 \text{ GeV}$.

Cut (1) suppresses the contamination of $b\bar{b}$ photoproduction where the heavy b quarks can undergo semi-leptonic decays. The transverse energy requirement in cut (2) is high enough to eliminate contamination from J/ψ photoproduction. Asking for two isolated e^- strongly suppresses the main DIS NC and photoproduction background, leaving only events where either a photon or a hadronic jet is misidentified as an e^- . Such a misidentified jet in DIS NC events is most probably found to be collinear with the true electron in the transverse plane. This can be seen in Fig. 7a where the azimuthal balance $\phi_{1,2}$ between the two e^- candidates found in the data is compared with SM Monte Carlo simulation. For this comparison with DIS NC, an additional cut of $2E_e^0 - P_z > 43 \text{ GeV}$ is imposed. The observed acollinearity in $\phi_{1,2}$ between the two e^- candidates is seen to be well described by the Monte Carlo.

The remaining background is suppressed with cut (3) and we are left with 26.1 ± 3.9 expected events from DIS NC while the photoproduction contamination is negligible. The estimated DIS NC background agrees well with the 28 observed events. This background is further suppressed by cut (4). The effect of this cut is seen in Fig. 7b showing Monte Carlo expectations for the correlation between $2E_e^0 - P_z$ and the azimuthal balance $\phi_{1,2}$ for DIS NC (plotted for $3 < L_{\text{data}} < 10$) and stop pair production (arbitrary normalization). Two events are rejected by cut (5).

With cuts (1) to (5), we are left with no observed event candidate while 1.0 ± 0.8 event is expected from misidentified DIS NC background. The detection efficiencies for the signal of $t\bar{t}$ pair production after all selection cuts are found to rise from about 3% at 9 GeV to 32% at 24 GeV.

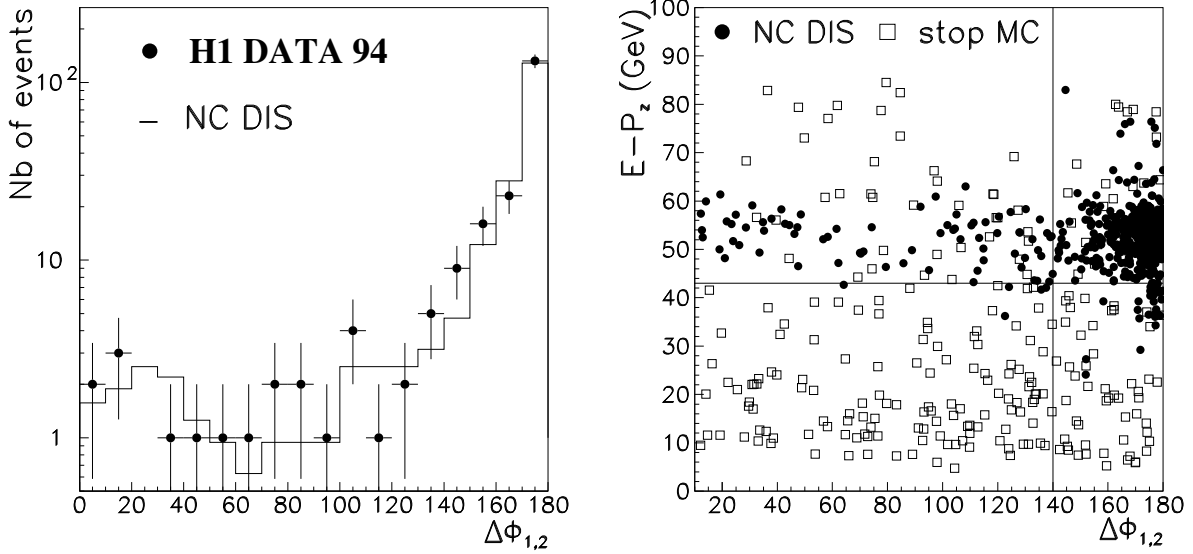


Figure 7: (a) Azimuthal balance $\Delta\Phi_{1,2}$ of the two e^- candidates for data (closed dots) and DIS Neutral Current Monte Carlo (histogram) when $(E - P_z) > 43 \text{ GeV}$. (b) Comparison of Monte Carlo expectations for the missing longitudinal momentum $(E - P_z)$ versus the balance in azimuth of the two e^- candidates $\Delta\Phi_{1,2}$ for DIS Neutral Current (closed dots) and stop pair production in gg -gluon fusion (open squares) for $M_t = 20 \text{ GeV}$.

5 Results

In the absence of significant deviation from the SM expectations, we now derive exclusion limits for the Yukawa couplings Y_{ijk}^0 as a function of mass, combining all contributing channels and making use of the number of observed events, of expected background events, and the signal detection efficiencies for each contributing channel.

Single production of squarks:

For the event topologies S1 to S3, the detection efficiencies are folded with a mass bin of variable width which slides over the accessible M_q range. The bin width is optimized taking into account the mean expected background and the expected q mass resolution and contains about 68% of the signal at a given mass, e.g. at 150 GeV we typically have a full bin width of $M_{e'} \sim 25 \text{ GeV}$ in S1, of $M_h \sim 35 \text{ GeV}$ in S2, and of $M_{dec} \sim 40 \text{ GeV}$ in S3. For event topologies S4 to S8 where the number of observed events and expected background is always < 10 , the signal is integrated above the selection cuts (i.e. without explicit restriction on the reconstructed mass). More details on the methodology for the limits derivation and on the procedure for folding the channel per channel statistical and systematic errors are given in [1].

The detection efficiencies have to be folded with the branching fractions in each of the possible event topologies, properly taking into account the relative production cross-

section of the various squark flavours (i.e. $\tilde{\alpha}_R$ and $\tilde{\alpha}_L$ for $\tilde{a}_{111} \neq 0$). For small $M_{\tilde{g}} = M_{\tilde{q}}$ and/or small \tilde{a}_{ijk} values where gauge decays of the squark are expected to dominate, the dependence upon the values of the free parameters of the MSSM has to be fully considered for the coupling constants at the $\tilde{q} \rightarrow q + \tilde{\chi}_1^0$ or $\tilde{q} \rightarrow q^0 + \tilde{\chi}_1^+$ vertex as well as the decay branchings of the $\tilde{\chi}_1^0$ and $\tilde{\chi}_1^+$. We will discuss our results in terms of the usual parameters: the ratio $\tan \beta$ of the two Higgs field vacuum expectation values, the higgsino mixing parameter μ , the mass parameter M_2 for the SU(2) gauginos.

The domains of the $(M_2; \mu)$ plane where decays into a specific neutralino or chargino dominate for the $\tilde{\alpha}_L$ are shown in Fig. 8a for a squark mass in the middle of the accessible $M_{\tilde{q}}$ range. The decay into the lightest chargino $\tilde{\chi}_1^+$ is seen to dominate as soon as kinematically

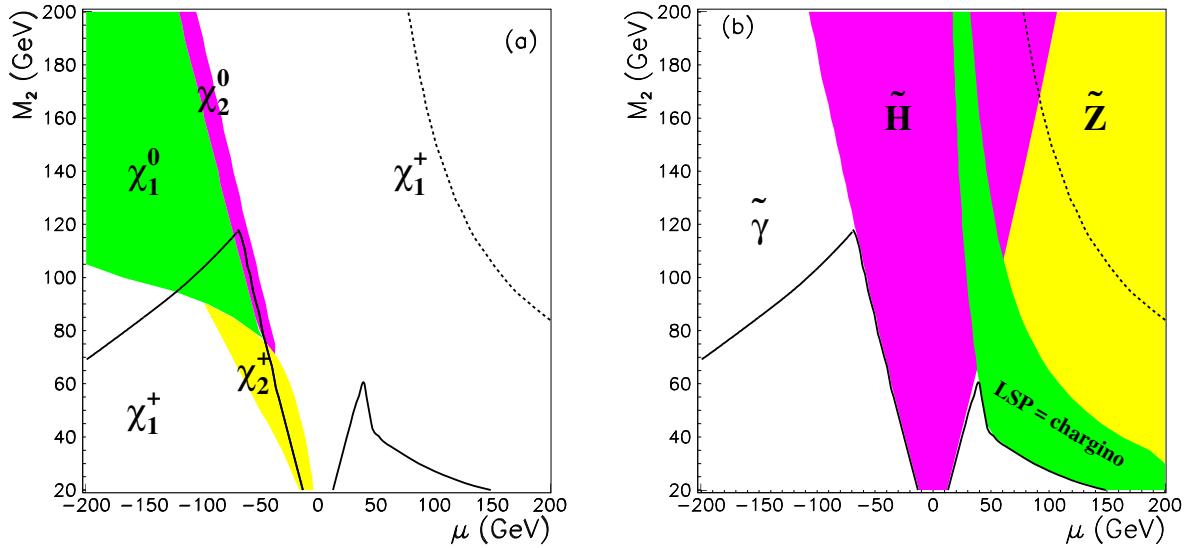


Figure 8: (a) Regions in the $M_2; \mu$ plane where a 150 GeV u_L squark decays dominantly into one of the $\tilde{\chi}_1^0$ or $\tilde{\chi}_1^+$ states for $\tan \beta = 1$; (b) Main component of the lightest neutralino in the plane $(M_2; \mu)$, for $\tan \beta = 1$. In (a) and (b) the region below the full curve corresponds to a domain in which the branching ratio of the $\tilde{\chi}_1^0$ into $e q\bar{q}^0$ is greater than 80%. Along the dotted curve, the branching into $e q\bar{q}^0$ is of about 20% for a $\tilde{\chi}_1^0$ of 20 GeV.

ically allowed. This is contrary to the $\tilde{\alpha}_R$ which mainly decays into $d + \tilde{\chi}_1^0$ (except when the $\tilde{\chi}_1^0$ is H^- -dominant). For a H^- -dominant LSP the coupling constant is small enough to suppress strongly squark gauge decays into $\tilde{\chi}_1^0$.

Regions for various kinds of $\tilde{\chi}_1^0$ in the parameter space are shown in Fig. 8b. Similar plots of the admixture of the weak eigenstates $\tilde{\gamma}, \tilde{Z}, \tilde{H}_1^0$ and \tilde{H}_2^0 in the neutralino LSP are given in [32]. In the region where the $\tilde{\chi}_1^0$ is $\tilde{\gamma}$ -like, the branching ratio of the $\tilde{\chi}_1^0$ into $e q\bar{q}^0$ is greater than 60% for $\tan \beta = 1$. When the $\tilde{\chi}_1^0$ is a pure $\tilde{\gamma}$ ($M_2 = 0$), this branching saturates at about 88%. In the region where the $\tilde{\chi}_1^0$ is \tilde{Z} -like, for instance along the dotted line for a $\tilde{\chi}_1^0$ of 20 GeV, the branching ratio into $e q\bar{q}^0$ is about 20%.

$M_{\bar{\nu}}; M_{\nu_1}^0$ (GeV)		S ₁	S ₂	S ₃	S ₄	S ₅	S ₆	S ₇	S ₈	ϵ^P "B
75 ; 40	N _{observed}	20	17	60	0	9	3	0	4	25.5 13.3 37.0
	N _{expected}	20.66	22.9	41.4	0.	3.9	4.07	0.76	2.4	
	B (~)	1.2	0.4	40.8	40.8	16.9	–	0	0	
	B (Z')	11.2	5.0	5.4	3.0	71.4	–	0.2	1.7	
	B (H')	89.9	10.0	0	–	0	0	–	–	
	" (~)	35.7	48.8	34.8	24.3	4.7	0	0	0	
150 ; 40	N _{observed}	3	8	5	0	9	3	0	4	20.1 28.2 21.0
	N _{expected}	1.62	8.58	2.71	0.	3.9	4.07	0.76	2.4	
	B (~)	3.4	1.0	26.6	7.2	17.0	–	7.5	1.5	
	B (Z')	7.3	1.8	16.7	0.5	45.0	–	0.7	5.8	
	B (H')	10.0	1.2	5.4	–	23.2	7.8	–	–	
	" (~)	45.5	54.2	33.1	20.9	32.8	51.0	23.1	29.8	
250 ; 40	N _{observed}	0	1	17	0	9	3	0	4	30.8 32.6 23.8
	N _{expected}	0.0	0.59	16.2	0.	3.9	4.07	0.76	2.4	
	B (~)	36.5	4.9	20.4	2.5	18.7	–	0.3	0.06	
	B (Z')	43.3	4.2	15.9	0.2	19.7	–	0.04	0.3	
	B (H')	45.6	4.3	4.2	–	0.6	0.2	–	–	
	" (~)	46.1	29.9	25.5	14.3	36.7	43.1	24.0	30.5	
150 ; 80	N _{observed}	3	8	6	0	9	3	0	4	41.4 46.1 17.6
	N _{expected}	1.62	8.58	3.48	0.	3.9	4.07	0.76	2.4	
	B (~)	23.1	1.2	26.3	26.3	23.0	–	0	0	
	B (Z')	80.0	1.6	1.9	1.9	14.5	–	0	0	
	B (H')	21.4	1.4	7.4	0	13.3	4.4	–	–	
	" (~)	45.5	54.2	42.9	27.0	51.6	36.5	0	0	
250 ; 80	N _{observed}	0	1	6	0	9	3	0	4	28.1 40.0 29.6
	N _{expected}	0.	0.59	3.10	0.	3.9	4.07	0.76	2.4	
	B (~)	52.1	4.4	2.5	1.8	2.2	–	0.3	0.13	
	B (Z')	56.5	4.3	9.6	0.06	14.1	–	0.04	1.41	
	B (H')	58.2	4.6	3.5	0	0.2	0.08	–	–	
	" (~)	46.1	29.9	36.3	20.3	58.6	33.0	44.5	44.7	

Table 4: Number of observed events, of expected background events and branching ratios B (in %) corresponding to channels S1 to S8 for some values of $M_{\bar{\nu}}$ and $M_{\nu_1}^0$, and presented for ~-like, Z'-like and H'-like ν_1^0 . The efficiencies ϵ^P are given in each channel for the ~-like case except for S6 where they are given for the H'-like case. Also given is the ϵ^P "B summed over all channels for each ν_1^0 type.

The relative contribution of each of the channels S1 to S8 is given in Table 4 for a few representative cases. For the chosen examples, the mass of the $\tilde{\chi}_1^+$ is about twice that of the $\tilde{\chi}_1^0$ except for heavy (e.g. 80 GeV) \tilde{H}^- -like $\tilde{\chi}_1^0$ for which $M_{\tilde{\chi}_1^+} \approx M_{\tilde{\chi}_1^0} \approx 1.3$. In the low squark mass region, the decay modes S3 and S4 dominate since the decay of the squark into $\tilde{\chi}_1^+$ is largely suppressed by phase space and since the Yukawa couplings probed are small. For medium masses, when the \tilde{q} is heavier than the $\tilde{\chi}_1^+$, it decays dominantly via S3 and S5. The channel S5 contributes mainly when the $\tilde{\chi}_1^0$ is \tilde{Z}' -like, since in that case the branching ratio for $\tilde{\chi}_1^0 \rightarrow \tilde{\chi}_1^+ + 2\text{jets}$ is generally above 70%. At very large \tilde{q} masses, we are only sensitive to high values of the coupling, so that the $\tilde{\chi}_p$ decay S1 into $e^+ + \text{jet}$ dominates whereas $\tilde{\chi}_p$ decays S2 are strongly suppressed by the parton density.

From the total branching fraction (i.e. summed over all above channels), it is inferred that the contribution of the decays into heavier $\tilde{\chi}_i^0$ ($i > 1$) and $\tilde{\chi}_j^+$ ($j > 1$) is generally small. Hence, in order to simplify the derivation of limits we have assumed conservatively that the \tilde{q} decay into these heavy states are allowed but measured with vanishingly small efficiencies. Folded in the derivation of limits are systematic errors coming from the uncertainty on the luminosity measurement (1.5%), the finite Monte Carlo statistics, the absolute energy calibration which leads to an uncertainty on the background estimation of about 10%, the choice of the scale entering the structure function calculation (which leads to 7% uncertainties in the cross-section) and the choice of the parton density parameterization.

The exclusion limits obtained on the coupling \tilde{g}_{111}^0 at 95% confidence level (CL) are shown in Fig. 9 as function of the \tilde{q} mass ($\tilde{\alpha}_L$ and $\tilde{\alpha}_R$) in the hypothesis that the $\tilde{\chi}_1^0$ is a pure $\tilde{\chi}$. The limits represent an improvement of about a factor two to three compared to our previously published results [1] at low squark masses. The gain from integrated luminosity is only partially cancelled by a less favourable quark density since for incident positron, the $e^+ d \rightarrow \tilde{\alpha}_L$ production dominates over $e^+ u \rightarrow \tilde{\alpha}_R$ whilst $e u \rightarrow \tilde{\alpha}_R$ dominates over $e d \rightarrow \tilde{\alpha}_L$ for incident electron data. The limits also improve at largest mass where the smaller coupling probed implies a narrow observable resonance width.

For the smallest couplings accessible here, a squark lighter than 230 GeV undergoes dominantly a gauge decay. Hence in contrast to earlier searches [1], we are here sensitive to event topologies immediately distinguishable from those of leptoquarks. The existence of first generation squarks with $\tilde{\chi}_p$ Yukawa coupling \tilde{g}_{111}^0 is excluded for masses up to 240 GeV (depending on the $\tilde{\chi}_1^0$ mass) at coupling strengths $\tilde{g}_{111}^0 = 4$ & \tilde{g}_{em} (up to 130 GeV for coupling strengths $\tilde{g}_{em} = 0.01$).

In the more general case, where the $\tilde{\chi}_1^0$ is a mixture of gauginos and higgsinos, the exclusion limits on the coupling \tilde{g}_{111}^0 at 95% CL are shown in Fig. 10 as function of the \tilde{q} mass. Here, the limits are derived for a reference point in the MSSM parameter space chosen as $\tilde{m}_0 = 160$ GeV and $M_2 = 60$ GeV for a $\tilde{\chi}$ -like $\tilde{\chi}_1^0$, $\tilde{m}_0 = 150$ GeV and $M_2 = 150$ GeV for a \tilde{Z}' -like $\tilde{\chi}_1^0$, and $\tilde{m}_0 = 44$ GeV and $M_2 = 140$ GeV for a \tilde{H}^- -like $\tilde{\chi}_1^0$. These points in the parameter space lie outside the domain excluded from the invisible Z_0 width measurement at LEP [33]. The rejection limits for a $\tilde{\chi}$ -like $\tilde{\chi}_1^0$ are found not to differ much from those obtained for pure $\tilde{\chi}$. The limits are also seen not to depend too strongly on the nature of the LSP. The three curves merge together at highest squark masses, where the branching of the squark into $\tilde{\chi}_1^0 q$ becomes negligible relative to $\tilde{\chi}_p$.

Figure 9: Exclusion upper limits at 95% C.L. for the coupling \tilde{g}_{111}^0 as a function of the squark mass for various fixed photino masses and derived for $\tan\beta = 1$. The regions above the curves are excluded. The limits combine $\tilde{\mathbb{B}}_p$ and gauge decays of the \tilde{d}_R and \tilde{u}_L .

decay. The limits obtained are found moreover not to depend strongly on the parameter $\tan\beta$. Varying $\tan\beta$ from 1 to 40, we find that the limits only slightly degrade and mainly at very low m_q masses, by 30% at $M_q = 45$ GeV down to 2% at 200 GeV.

From the analysis of the \tilde{g}_{111}^0 case involving the \tilde{d}_R and \tilde{u}_L squarks, limits can be deduced on the \tilde{g}_{1jk}^0 by folding in the proper parton densities. Such limits are given in Table 5 at $M_q = 150$ GeV. For $M_q \gtrsim 150$ GeV, the exclusion limits for \tilde{g}_{111}^0 and \tilde{g}_{121}^0 in particular are found to coincide within 5%.

Our rejection limits extend considerably beyond the only other collider limits of $M_q > 100$ GeV for \tilde{g}_{111}^0 inferred in [30] from dilepton data of the Tevatron experiments. Moreover, this Tevatron limit was derived only under the restrictive assumption that the LSP is the $\tilde{\chi}_0$ and that squarks other than the stop are degenerate in mass. If one assumes that one squark is substantially lighter than the others, this bound is much weaker [2] and only slightly above the mass reach of LEP 1. On the contrary, our \tilde{g}_{111}^0 coupling limits only weakly depend on the mass degeneracy assumption since, as mentioned above, the \tilde{u} production strongly dominates. Hence, if the first generation \tilde{u} is significantly lighter than other squarks, we probe here (and similarly for the \tilde{d} in [1]) a large portion of the mass-coupling domain unexplored by other experiments.

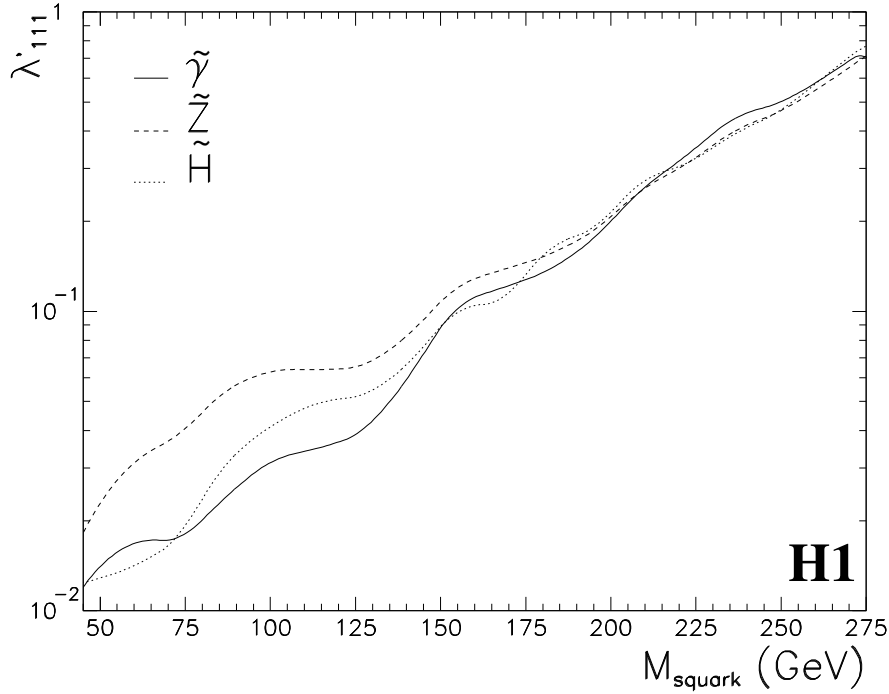


Figure 10: Exclusion upper limits at 95% CL for the coupling λ_{111}^0 as a function of squark mass for different natures of the $\tilde{0}_1$ for $M_{\tilde{0}_1} = 40$ GeV and for $\tan\beta = 1$ (region above the curve excluded). The full curve corresponds to cases where the LSP is $\tilde{\gamma}$ -like, the dotted one to a \tilde{H} -dominant LSP and the dashed one to a \tilde{Z} -like LSP.

There are no other direct limits published for λ_{1jk}^0 (j or $k \neq 1$). This is particularly interesting since indirect limits for this coupling are also weaker [2] than those [35] for λ_{111}^0 .

Production of stop squarks:

For the derivation of exclusion limits for the pair production of stop squarks, a 15% uncertainty on the cross-section (which varies from $\sigma_{\text{stop}} = 200$ pb at 9 GeV to $\sigma_{\text{stop}} = 1$ pb at 24 GeV) is due to the specific choice of gluon density. The uncertainty was determined by comparing with MRSD [15] and constitutes the main source of systematic error.

The exclusion limit obtained on the stop mass at 95% CL is shown in Fig.11. A stop in the range $9 < M_{\tilde{t}_1} < 24.4$ GeV is excluded at 95% CL. This limit does not depend upon the value of λ_{13k}^0 (as far as $\lambda_{13k}^0 \cos\theta_t \gtrsim 10^{-4}$, below which value the decay into c and $\tilde{0}_1$ cannot be neglected anymore). The angle θ_t is the mixing angle in the mass matrix of the stop (see for example [36]).

If the coupling λ_{131}^0 dominates, the stop can be singly produced in reactions of the type $e^+ + d \rightarrow \tilde{t}$. Under our phenomenological assumptions (see section 2) and as long

Table 5: Exclusion upper limits at 95% CL on the couplings \tilde{g}_{1jk}^0 for $M_{\tilde{q}} = 150 \text{ GeV}$ and $M_{\tilde{g}} = 80 \text{ GeV}$. The quoted values for \tilde{g}_{111}^0 are given for $\tilde{\chi}$ -dominant and for Z' -dominant \tilde{g}_1^0 . In other cases, the higgsino component of the \tilde{g}_1^0 is assumed to be vanishingly small. Moreover, the results for cases with $j = 3$ are only valid under the additional restriction that $M_{\tilde{t}_1} > M_{\tilde{q}}$.

\tilde{g}_{1jk}^0	$\tilde{g}_{\text{lim}}^0 \sim \text{case}$	$\tilde{g}_{\text{lim}}^0 Z' \text{ case}$
\tilde{g}_{111}^0	0.056	0.048
\tilde{g}_{112}^0	0.14	0.12
\tilde{g}_{113}^0	0.18	0.15
\tilde{g}_{121}^0	0.058	0.048
\tilde{g}_{122}^0	0.19	0.16
\tilde{g}_{123}^0	0.30	0.26
\tilde{g}_{131}^0	0.06	0.05
\tilde{g}_{132}^0	0.22	0.19
\tilde{g}_{133}^0	0.55	0.48

as $(\tilde{g}_{131}^0 \cos \theta_t) \lesssim 10^{-4}$, the search of the \tilde{t} borrows from the analysis for \tilde{B}_p decays of first generation squarks. We find that masses below 138 GeV are excluded at 95% CL for coupling strength of $(\tilde{g}_{131}^0 \cos \theta_t)^2 = 4 \lesssim 0.01_{\text{em}}$. This represents an increase of sensitivity of about an order of magnitude compared to our previous results [1]. As a comparison with other experiments, a \tilde{t} lighter than 38 GeV is excluded at 95% CL from LEP data [37] for $\theta_t = 0$ from the width of the Z_0 . But for θ_t close to the value for which the Z_0 decouples from the stop ($0.7 < \theta_t < 1.4$) there are no existing limit from LEP for \tilde{B}_p stops.

The coupling limit in Fig. 11 is extended beyond $M_{\tilde{t}} > M_{\text{top}}$. This portion of the exclusion limit curve is only valid for $M_{\tilde{t}} < M_{\text{top}} + M_{\tilde{g}_1^0}$.

6 Conclusions

We have searched for squarks from R-parity violating supersymmetry. The search was carried out for the first time at HERA in all possible decay processes allowed when wandering in the parameter space of the Minimal Supersymmetric Model. No significant evidence for the production of squarks was found and mass dependent limits on the couplings were derived. The existence of first generation squarks at masses up to 240 GeV are excluded at 95% confidence level for a strength of the Yukawa coupling \tilde{g}_{111}^0 of $\tilde{g}_{111}^0 = 4 \lesssim 0.01_{\text{em}}$. The limits extend far beyond results obtained at other colliders where our excluded domain in the mass-coupling plane for masses $\lesssim 100 \text{ GeV}$ has never been explored.

Scalar stop squarks were searched in pair and single production modes. The existence of light scalar stops with \tilde{g}_{13k}^0 couplings to light fermions is excluded for masses $9 < m_{\tilde{t}} < 24.4 \text{ GeV}$ at 95% confidence level. Stop squarks with \tilde{g}_{131}^0 couplings are excluded below 138 GeV at 95% confidence level for couplings $(\tilde{g}_{131}^0 \cos \theta_t)^2 = 4 \lesssim 0.01_{\text{em}}$.

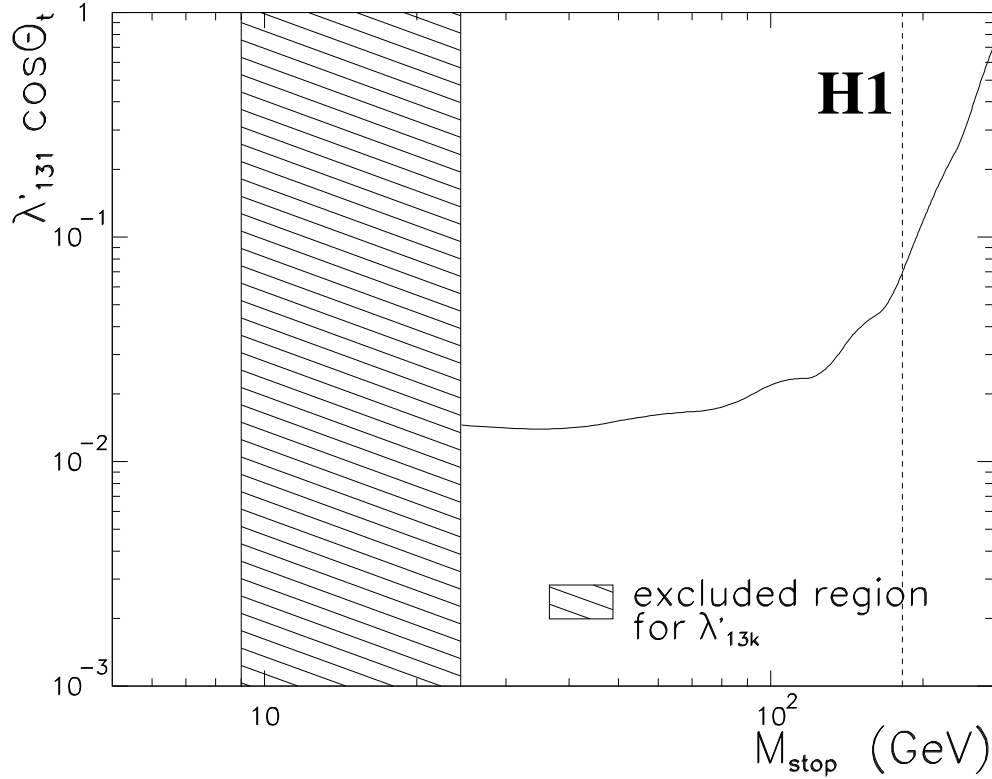


Figure 11: Exclusion limits for the coupling $\lambda'_{131} \cos \theta_t$ as function of the stop mass. The exclusion curve is obtained from the single stop production (region above the curve excluded). Beyond the dashed line, the limits are only valid for $M_t < M_{\text{top}} + M_{\chi_1^0}$. The hatched domain is excluded by the pair production search and concerns λ'_{13k} with $k = 1, 2$.

Acknowledgements

We wish to thank the HERA machine group as well as the H1 engineers and technicians who constructed and maintained the detector for their outstanding efforts. We thank the funding agencies for their financial support. We wish to thank the DESY directorate for the support and hospitality extended to the non-DESY members of the collaboration.

References

- [1] H1 Collaboration, T. Ahmed et al., Z. Phys. C 64 (1994) 545.
- [2] J. Butterworth and H. Dreiner, Nucl. Phys. B 397 (1993) 3, and references therein.
- [3] H1 Collaboration, S. Aid et al., Phys. Lett. B 369 (1996) 173.
- [4] W. Buchmüller, R. Ruckl and D. Wyler, Phys. Lett. B 191 (1987) 442.

- [5] E. Perez and Y. Sirois, "SU SY Searches at HERA ", To be published in the Proceedings of the International Workshop on Supersymmetry and Unification of Fundamental Interactions, Editions Frontieres (I. Antoniadis and H. V. Videau, Editors), (May 1995, Palaiseau).
- [6] E. Perez, "Recherche de Particules en Supersymetrie Violant la R-parite dans H1 a HERA ", These de Doctorat, DAPNIA/SPP report (in French), to be published.
- [7] J.F. Gunion and H.E. Haber, Nucl. Phys. B 272 (1986) 1.
- [8] T. Kon, T. Kobayashi and S. Kitamura, Phys. Lett. B 333 (1994) 263; T. Kon et al., Z. Phys. C 61 (1994) 239.
- [9] H1 Collaboration, I. Abt et al., "The H1 Detector at HERA ", DESY preprint 93-103 (July 1993) 194pp; idem DESY Internal Report H1-96-01 (March 1996) 157pp.
- [10] H1 Calorimeter Group, B. Andrieu et al., Nucl. Instr. and Meth. A 336 (1993) 460.
- [11] H1 Calorimeter Group, B. Andrieu et al., Nucl. Instr. and Meth. A 350 (1994) 57; idem, Nucl. Instr. and Meth. A 336 (1993) 499.
- [12] LEGO 0.02 and SUSSEX 1.5; K. Rosenbauer, Doktor Dissertation, RWTH Aachen (in German), PITHA 95/16 (July 1995).
- [13] PYTHIA 5.6; T. Sjöstrand, Comp. Phys. Comm. 39 (1986) 347; T. Sjöstrand and M. Bengtsson, Comp. Phys. Comm. 43 (1987) 367.
- [14] JETSET 7.3; T. Sjöstrand, CERN preprint TH-6488-92 (May 1992) 284pp.
- [15] A.D. Martin, W.J. Stirling and R.G. Roberts, Phys. Rev. D 47 (1993) 867.
- [16] A.D. Martin, R.G. Roberts and W.J. Stirling, Durham Univ. preprint DTP-93-86 and Rutherford Appleton Lab. preprint RAL-93-077 (October 1993) 16pp.; (PDFLIB [17] nucleon structure function type 1, group 3, set 36) .
- [17] H. Plothom-Besch, CERN-PPE Parton Density Functions program W 5051.
- [18] A. Bartl, H. Fraas and W. Majerotto, Z. Phys. C 30 (1986) 441.
- [19] DJANGO 2.1; G.A. Schuler and H. Spiesberger, Proceedings of the Workshop Physics at HERA, W. Buchmüller and G. Ingelman (Editors), (October 1991, DESY-Hamburg), vol. 3 p. 1419.
- [20] LEPTO 6.1; G. Ingelman, Proceedings of the Workshop Physics at HERA, W. Buchmüller and G. Ingelman (Editors), (October 1991, DESY-Hamburg), vol. 3 p. 1366.
- [21] HERACLES 4.4; A. Kwiatkowski, H. Spiesberger and H.-J. Mohring, Comput. Phys. Commun. 69 (1992) 155.
- [22] ARIADNE 4.0; L. Lonnblad, Comput. Phys. Commun. 71 (1992) 15.
- [23] JETSET 7.4; T. Sjöstrand, Lund Univ. preprint LU-TP-95-20 (August 1995) 321pp; idem, CERN preprint TH-7112-93 (February 1994) 305pp.
- [24] H1 Collaboration, I. Abt et al., Nucl. Phys. B 407 (1993) 515, ZEUS Collaboration, M. Derrick et al., Phys. Lett. B 316 (1993) 412.

- [25] M. Glück, E. Reya and A. Vogt, Phys. Rev. D 45 (1992) 3986; *idem*, Phys. Rev. D 46 (1992) 1973; (PDFLIB [17] nucleon structure function type 1, group 5 set 4; photon structure function type 3 group 5 set 3).
- [26] H1 Collaboration, B. Andrieu et al., Nucl. Inst. and Meth. A 344 (1994) 492.
- [27] H1 Collaboration, T. Ahmed et al., "Observation of an $e^+p \rightarrow X$ Event with High Transverse Momenta at HERA", DESY preprint 94-248 (December 1994) 9pp.
- [28] U. Baur, J.A.M. Vermaseren, D. Zeppenfeld, Nucl. Phys. B 375 (1992) 3.
- [29] In the course of completing this paper, we became aware of an alternative \mathbb{R}_p SUSY interpretation of the observed $e^+p \rightarrow X$ event candidate proposed by T. Kon, T. Kobayashi and S. Kitamura, Seikei Univ. preprint ITP-SU-96/02 (Tokyo, January 1996) 8pp.
There the event is discussed in terms of the single production of a scalar top squark through a g_{131}^0 coupling. The process $e^+p \rightarrow b_1^+ \rightarrow b^+ \tilde{g}_1^0$ with a stable \tilde{g}_1^0 would lead to a signature similar to that of our S6 channel. The process $e^+p \rightarrow b_1^+ \rightarrow b^+ \tilde{g}_1^0 \rightarrow b^+ b\bar{d}$ would lead to a signature similar to that of our S8 channel.
- [30] D.P. Roy, Phys. Lett. B 283 (1992) 270.
- [31] V. Barger, G.F. Giudice and T. Han, Phys. Rev. D 40 (1989) 2987.
- [32] H. Dreiner and P. Morawitz, Nucl. Phys. B 428 (1994) 31.
- [33] ALEPH Collaboration, D. Buskulic et al., Phys. Lett. B 349 (1995) 238.
- [34] M. Drees and K. Grassie Z. Phys. C 28 (1985) 451.
- [35] M. Hirsch, H.V. Klapdor-Kleingrothaus and S.G. Kovalenko, Phys. Rev. Lett. 75 (1995) 17.
- [36] T. Kon, T. Kobayashi and S. Kitamura, Phys. Lett. B 333 (1994) 263.
- [37] OPAL Collaboration, P.D. Acton et al., Phys. Lett. B 337 (1994) 207.

